



**HAL**  
open science

# Severe offtarget effects following intravenous delivery of AAV9-MECP2 in a female mouse model of Rett syndrome

Valerie Matagne, Emilie Borloz, Yann Ehinger, Lydia Saidi, Laurent Villard,  
Jean-Christophe Roux

## ► To cite this version:

Valerie Matagne, Emilie Borloz, Yann Ehinger, Lydia Saidi, Laurent Villard, et al.. Severe offtarget effects following intravenous delivery of AAV9-MECP2 in a female mouse model of Rett syndrome. *Neurobiology of Disease*, 2021, 149, pp.105235. 10.1016/j.nbd.2020.105235 . hal-03149051

**HAL Id: hal-03149051**

**<https://amu.hal.science/hal-03149051>**

Submitted on 3 Feb 2023

**HAL** is a multi-disciplinary open access archive for the deposit and dissemination of scientific research documents, whether they are published or not. The documents may come from teaching and research institutions in France or abroad, or from public or private research centers.

L'archive ouverte pluridisciplinaire **HAL**, est destinée au dépôt et à la diffusion de documents scientifiques de niveau recherche, publiés ou non, émanant des établissements d'enseignement et de recherche français ou étrangers, des laboratoires publics ou privés.



Distributed under a Creative Commons Attribution - NonCommercial 4.0 International License

1 SEVERE OFFTARGET EFFECTS FOLLOWING INTRAVENOUS DELIVERY of AAV9-MECP2 IN A FEMALE  
2 MOUSE MODEL OF RETT SYNDROME

3

4

5 Valerie Matagne\*, Emilie Borloz\*, Yann Ehinger, Lydia Saidi, Laurent Villard, Jean-Christophe Roux.  
6 Aix Marseille Univ, INSERM, MMG, U1251, Faculté de médecine Timone, 13385, Marseille, France

7

8

9

10 Corresponding author:

11 Jean-christophe.roux@univ-amu.fr

12 Tel: +33 4 91 32 49 04

13 Fax: +33 4 91 80 43 19

14

15

16 Present address for

17 YE: Departement of Neurology, University of California, San Francisco, CA USA

18 yann.ehinger@ucsf.edu

19 LS: Department of Psychiatry and Neuroscience, Faculty of medicine, Centre de recherche CERVO,  
20 Université Laval, 2601, Canardière, Room F-6500, Quebec City, QC, Canada

21

22

23 \* These authors contributed equally to this work

24

25

26

27

28

29

30

31

32

33

34

35

1 ABSTRACT

2

3 Rett syndrome (RTT) is a severe X-linked neurodevelopmental disorder that is primarily caused by  
4 mutations in the methyl CpG binding protein 2 gene (*MECP2*). RTT is the second most prevalent  
5 genetic cause of intellectual disability in girls, and there is currently no cure for the disease. We have  
6 previously shown that gene therapy using a self-complementary AAV9 viral vector expressing a  
7 codon-optimized *Mecp2* version (AAV9-MCO) significantly improved symptoms and increased  
8 survival in male *Mecp2*-deficient mice. Here, we pursued our studies and investigated the safety and  
9 efficacy of long-term gene therapy in the genetically relevant RTT mouse model: the heterozygous  
10 (HET) *Mecp2* deficient female mouse. These mice were injected with the AAV9-MCO through the tail  
11 vein and an array of behavioral tests was performed. At 16- and 30-weeks post-injection, this  
12 treatment was able to rescue apneas and improved the spontaneous locomotor deficits and  
13 circadian locomotor activity in *Mecp2* HET mice treated with AAV9-MCO at a dose of  $5 \times 10^{11}$   
14 vg/mouse.

15 To examine whether a higher dose of vector could result in increased improvements, we injected  
16 *Mecp2* HET mice with a higher MCO vector dose ( $10^{12}$  vg/mouse), which resulted in some severe,  
17 sometimes lethal, side effects. In order to confirm these effects, a new cohort of *Mecp2* HET mice  
18 were administered increasing doses of MCO vector ( $10^{11}$ ,  $5 \times 10^{11}$  and  $10^{12}$  vg/mouse). Again, two  
19 weeks after vector administration, some *Mecp2* HET mice were found dead while others displayed  
20 severe side effects and had to be euthanized. These deleterious effects were not observed in *Mecp2*  
21 HET mice injected with a high dose of AAV9-GFP and were directly proportionate to vector dosage (0,  
22 23 or 54% mortality at an AAV9-MCO dose of  $10^{11}$ ,  $5 \times 10^{11}$ ,  $10^{12}$  vg/mouse, respectively), and no such  
23 lethality was observed in wild-type (WT) mice.

24 In the *Mecp2* HET mice treated with the high and medium AAV9-MCO doses, blood chemistry  
25 analysis and post-mortem histology showed liver damage with drastically elevated levels of liver  
26 transaminases and disorganized liver architecture. Apoptosis was confirmed by the presence of  
27 TUNEL- and cleaved-caspase 3-positive cells in the *Mecp2* HET mice treated with the higher doses of  
28 AAV9-MCO. We then studied the involvement of the unfolded protein response (UPR) in triggering  
29 apoptosis since it can be activated by AAV vectors. Increased expression of the C/EBP homologous  
30 protein (CHOP), one of UPR downstream effectors, was confirmed in *Mecp2* HET mice after vector  
31 administration.

32 The toxic reaction seen in some treated mice indicates that, although gene therapy for RTT improved  
33 breathing deficits observed in *Mecp2* HET mice, further studies are needed to better understand the

1 underlying mechanisms and caution must be exercised before similar attempts are undertaken in  
2 female Rett patients.

3

4 Keywords: Rett syndrome, Mecp2, AAV9, Gene therapy, Animal models, side effects.

5

## 1 INTRODUCTION

2 Rett syndrome (RTT) is a severe X-linked neurodevelopmental disorder that is primarily caused by  
3 mutations in the methyl CpG binding protein 2 gene (*MECP2*) (Amir et al., 1999) and is the second  
4 most prevalent genetic cause of intellectual disability in girls (Hagberg, 1995; Naidu, 1997; Neul et al.,  
5 2010). It is a disease affecting not only the CNS (profound cognitive and motor deficits) but also  
6 motor and autonomic functions (including severe breathing abnormalities). Currently, treatments are  
7 aimed at alleviating symptoms and there is no cure for RTT (Katz et al., 2012; Lombardi et al., 2015).

8 *Mecp2* is a transcription factor and a genome-wide regulator of chromatin structure [see (Lyst and  
9 Bird, 2015) for review] that was also involved in many other pathways including miRNA processing  
10 (Samaco and Neul, 2011), mRNA splicing (Cheng et al., 2017), oxidative stress [reviewed in (Müller,  
11 2019)] and neuronal network connectivity (Sun et al., 2019, 2019). A large amount of literature  
12 highlights the complexity of *Mecp2*'s molecular and cellular functions and explains why therapeutic  
13 approaches other than replacing *MECP2* may only partially improve RTT symptoms.

14 In recent years, significant progress was made in the field of CNS gene therapy (Hocquemiller et al.,  
15 2016), in part due to the use of the adeno-associated virus 9 (AAV9) that is capable of crossing the  
16 blood brain barrier and transduce brain cells after intravenous injection (Duque et al., 2009; Foust et  
17 al., 2009; Gray et al., 2011). These advances, together with the fact that reversal of neurological  
18 symptoms was possible in adult diseased RTT mice (Guy et al., 2007), indicated that *Mecp2* gene  
19 therapy might be beneficial for RTT patients. Using slightly different AAV9 therapeutic vectors, three  
20 teams showed that gene therapy resulted only in moderated improvement in RTT male mouse  
21 neurological phenotypes and lifespan (Gadalla et al., 2013; Garg et al., 2013; Matagne et al., 2017).

22 Although most RTT studies are carried out in male RTT mouse models for practical reasons (shorter  
23 endpoints, more robust phenotype), the heterozygous (HET) *Mecp2* female mouse is the most  
24 relevant genetic model of RTT and it also displays a robust phenotype, albeit milder and later than in  
25 males [reviewed in (Katz et al., 2012)]. There is so far only one study reporting improvement in RTT  
26 symptoms after gene therapy in female HET *Mecp2* mice (Garg et al., 2013). Here, we studied the  
27 effect of gene therapy in the female RTT mouse in order to obtain more preclinical data on the safety  
28 and efficacy of long-term treatment.

29

## 1 RESULTS

### 2 *Long term effect of AAV9-MCO: improvement of breathing pattern and locomotor deficits*

3 To examine the therapeutic effect of AAV9-mediated gene therapy, we treated *Mecp2* heterozygous  
4 (HET) female mice with a self-complementary AAV9 vector expressing a codon optimized *Mecp2*  
5 (AAV9-MCO) that was previously shown to have a beneficial effect in the *Mecp2-deficient* male mice  
6 (Matagne et al., 2017). Based on these results, we injected 5-month-old symptomatic *Mecp2* HET  
7 mice (Samaco et al., 2013) through the tail vein with AAV9-MCO (MCO) at a dose of  $5 \times 10^{11}$   
8 vg/mouse. All mice were tested for breathing deficits, sensorimotor coordination and locomotor  
9 activity one week before vector administration in order to get their baseline levels, and then 8, 16  
10 and 30 weeks post-injection (Figure 1).

11 As a summary, radar chart in Figure 1B and C exemplify the performance of each group across  
12 representative phenotypic variables at 1 week before viral vector administration and 30 weeks after  
13 viral vector administration, respectively. While the HET and HET MCO MED groups showed similar  
14 phenotypic profiles at the beginning of the study (Figure 1B), the HET MCO MED group displayed  
15 improved parameters compared to the HET group at the end of the study (Figure 1C).

16 At the age of 5 months, *Mecp2* HET mice already presented a significant increase in the number of  
17 apneas and alteration in breathing pattern as shown by a significantly different mean frequency and  
18 variability when compared to WT mice (Table 1). These *Mecp2* HET mice were then randomly  
19 assigned to the control (vehicle) or the AAV9-MCO treated group and assessed for breathing deficits.  
20 While the number of apneas stayed significantly higher in the *Mecp2* HET group throughout the  
21 study (Figure 1D), it steadily decreased in *Mecp2* HET MCO throughout testing and reached  
22 significance at 16 weeks post-administration. At this time, the untreated *Mecp2* HET group showed  
23 significant decrease in ventilation and increase in mean frequency while the *Mecp2* HET MCO mice  
24 showed trends to a normalization of these parameters (Table2). These results indicate that the AAV9-  
25 MCO treatment was able to rescue (number of apneas) or improve (ventilation and mean frequency)  
26 *Mecp2* HET mice breathing deficits.

27 Sensorimotor activity, measured by performance on the Rotarod test, was slightly decreased in the  
28 *Mecp2* HET group at the beginning of the study (Table 3, Figure 1E) and reached significance in  
29 ulterior tests. No improvement was observed in the *Mecp2* HET MCO group (Figure 1E).

30 Spontaneous locomotor activity was assessed in the open field test. Throughout the study, in *Mecp2*  
31 HET mice, there was a significant decrease in distance, velocity, activity and vertical activity (Table 3,  
32 Figure 1F-I). While, in the *Mecp2* HET MCO group, there seemed to be tendency to a normalization of  
33 these parameters at the end of the study (Figure 1F-I).

34 Because disruptions in circadian rhythm were reported in different Rett mouse models (Li et al.,  
35 2015; Tsuchiya et al., 2015), we used a home cage monitoring system to study the daily circadian

1 locomotor activity in *Mecp2* HET mice. At 5 months of age, *Mecp2* HET mice showed the same daily  
2 level of activity but travelled shorter distance than their WT counterparts (Figure 2A).  
3 At 30 weeks post-treatment, 12-month-old *Mecp2* HET mice still showed a decrease in distance  
4 travelled when compared to the WT group, while the *Mecp2* HET MCO group showed a trend to  
5 normalization (Figure 2B-C).  
6 These results show that AAV9-MCO treatment improves locomotor deficits in *Mecp2* HET mice in  
7 short (Open field) and long duration (home cage) assessments.  
8  
9 *AAV9-MCO administration in Mecp2 HET mice causes acute liver toxicity in a dose dependent*  
10 *manner.*  
11 Although the number of apneas was significantly decreased after MCO administration, all other  
12 measured parameters showed little improvement. To examine whether a higher dose of vector could  
13 result in increased improvements, we injected *Mecp2* HET mice with a high MCO vector dose ( $10^{12}$   
14 vg/mouse, n=4). Two weeks post vector administration, two mice were found dead (Table 4, group  
15 #2). In order to verify whether this occurrence happened by chance or was due to the vector  
16 administration, we injected *Mecp2* HET mice with the high MCO vector dose or the previous dose  
17 used as a control (Medium/MED MCO vector dose of  $5 \times 10^{11}$  vg/mouse, n=5 for each group; Table 4,  
18 group #3). Again, in the HET MCO High group, 3 mice were found dead and 2 showed severe side  
19 effects and had to be euthanized. While there were no observed death nor deleterious side effects in  
20 the first HET MCO MED group tested (Table 4, group #1), in this second group, one mouse was found  
21 dead and 2 mice were ill and had to be euthanized. Because of the deleterious side effects observed,  
22 we decided that these had to be investigated before any long-term phenotypical study could be  
23 pursued. All surviving mice were therefore sacrificed at that time (2 weeks post-administration) and  
24 blood and tissue samples were kept for post-mortem analysis. In addition to these mice, a new group  
25 of *Mecp2* HET mice was injected with 3 doses of AAV9-MCO (MED and High MCO vector doses  
26 already tested and a low MCO vector dose of  $10^{11}$  vg/mouse deemed safe, Table 4, group #4), as well  
27 as a group of WT mice injected with the 3 doses of AAV9-MCO (Table 4, group #5). We also included  
28 a group of mice injected with a high dose of the control AAV9-GFP vector (AAV9-GFP, n=8 HET and  
29 n=7 WT) to parse out the effect of the AAV9 vector from that of the transgene (Table 4, group #6).  
30 In these last AAV9-MCO injected cohort, there were no early death observed in either HET or WT  
31 mice. Overall, there was a total of 7/13 dead mice (54% mortality) in the HET MCO HIGH group and  
32 3/13 dead mice (23% mortality) in the HET MED MCO group.  
33 Mice were sacrificed 2 weeks post injection and serum markers for general (LDH, lactate  
34 dehydrogenase) and specific tissue damage in liver (ALT and AST, aspartate and alanine

1 transaminase, respectively), heart (CK, creatine kinase) and kidney (creatinine, urea) were quantified.  
2 These markers were chosen because of the natural tropism of the AAV9 vector for the heart, liver  
3 and, to a lesser extent, kidney (Chen et al., 2015).

4 Examination of blood chemistry markers the AAV9-MCO groups (WT MCO HIGH, HET MCO MED and  
5 HIGH) revealed a significant elevation in LDH (Suppl figure 1A), proof of tissue injury. Measurement  
6 of specific tissue damage markers showed that the heart and kidneys did not seem to be affected (no  
7 significant increase in CK, creatinine or urea, Suppl figure 1B-D) while significant increases in ALT and  
8 AST indicated some liver damage (Figure 3A-B) in both MCO-injected *Mecp2* HET and WT mice.  
9 Interestingly, ALT levels were also significantly elevated in untreated *Mecp2* HET mice compared to  
10 the WT ones (73.91±14.15 in HET, n=7 vs 29.68±4.96 in WT, n=7, \*\* p=0,026 Mann-Whitney Rank  
11 Sum Test).

12 In the AAV9-GFP injected groups, mice appeared healthy, which was confirmed by the absence of  
13 any significant increase in all measured serum markers (Suppl Figure 2A-C). Liver integrity was  
14 assessed by hematoxylin-eosin (H&E) staining in both AAV9-GFP and AAV9-MCO injected mice.  
15 Compared to control (Figure 3C-D, Suppl Figure 2D,F), liver sections showed no gross anomalies in  
16 WT and *Mecp2* HET mice injected with the AAV9-GFP vector (Suppl Figure 2E,G, respectively). AAV9-  
17 MCO injected WT did not display any liver injury (Figure 3E,G), while HET MCO MED and HIGH mice  
18 (Figure 3F,H respectively) showed clear liver damage characterized by lymphocyte infiltration and  
19 apoptotic cells. Hepatic toxicity was variable in the HET MCO MED group as H&E staining revealed  
20 medium to severe liver damage (Figure 3F and Suppl figure 3). Apoptosis was confirmed by a TUNEL  
21 staining assay in the HET MCO High (Figure 4F) while no apoptotic cells were identified in the HET  
22 MCO LOW and MED groups (Figure 4D-E). The presence of cleaved Caspase-3 immunopositive cells  
23 further confirmed the occurrence of apoptosis in the HET MCO MED and HIGH groups (Figure 4J-K)  
24 compared to the HET control group (Figure 4H).

25

#### 26 *AAV9-mediated transgene expression depends on both mouse genotype and type of transgene*

27 Immunostaining for GFP (Figure 5A-D) showed that the AAV9-GFP vector did target the liver of both  
28 WT and *Mecp2* HET mice, confirming that the absence of toxicity of the control viral vector was not  
29 due to a lack of transduction efficacy. Moreover, there was a higher GFP intensity staining in the  
30 *Mecp2* HET GFP group compared to the WT GFP group (n=3 and 6, respectively, 1.6 fold increase,  
31 p=0.0044 Mann-Whitney rank sum test). This difference was verified by western blot (Figure 5E) that  
32 showed a 4.3 fold increase in GFP expression when comparing the *Mecp2* HET GFP and WT GFP  
33 groups (p=0.009, Mann-Whitney rank sum test, n= 6).

34 In the AAV9-MCO injected WT groups, there was a dose dependent increase in the levels of *Mco*  
35 vector DNA (Figure 6A) that did not translate into increasing levels of *Mco* cDNA since the lowest

1 AAV9-MCO dose resulted in the highest *Mco* cDNA levels (Figure 6B). However, this did not affect  
2 *Mecp2* protein expression that also followed a dose-dependent pattern (Figure 6C). In the *Mecp2*  
3 HET MCO groups, there was a dose-dependent expression of *MCO* DNA, cDNA and *Mecp2* protein  
4 (Figure 6A-C). Although both vector DNA and cDNA levels tended to be higher in the *Mecp2* HET mice  
5 compared to the WT ones at the highest AAV9-MCO dose, this difference tended to reverse itself at  
6 the protein level.

7

#### 8 *Accumulation of the MCO transgene and activation of the UPR cascade*

9 While we observed similar *Mco* cDNA levels in AAV9-MCO injected WT and *Mecp2* HET mice, the  
10 lower levels of *Mecp2* protein in the *Mecp2* HET MCO MED and HIGH groups led us to wonder  
11 whether there was a disruption in the mRNA translation pathway. To answer this question, we  
12 looked at the unfolded protein response (or UPR), which is a cytoprotective signaling pathway  
13 activated by endoplasmic reticulum (ER) stress and that has previously been found to be triggered by  
14 AAV vectors (Balakrishnan et al., 2013). Using qPCR (Figure 7), we measured the mRNA levels of *Bip*  
15 (Binding immunoglobulin protein), the master regulator of the UPR pathway, and three downstream  
16 transcripts: *Chop* (C/EBP homologous protein), *IRE1* (inositol-requiring enzyme 1) and *ATF6*  
17 (activating transcription factor 6). In the liver of *Mecp2* HET MCO mice, there was a trend in higher  
18 *Bip* mRNA levels (Figure 7A,  $p=0.056$  Kruskal-Wallis One Way Analysis of Variance on Ranks) and a  
19 significant increase in *CHOP* mRNA at the AAV9-MCO medium dose (Figure 7B). A similar increase in  
20 *CHOP* mRNA was also observed in the WT MCO HIGH group. We did not observe any significant  
21 changes in the 2 other downstream UPR elements (IRE1 and ATF6) after AAV9-MCO administration in  
22 either WT or *Mecp2* HET mice (Figure 7C, D). The increase in CHOP levels was also confirmed by  
23 western blot (Figure 7E). Although very variable, there was an increase in CHOP levels in both WT  
24 and *Mecp2* HET MCO mice injected with the AAV9-MCO vector that only reached significance in the  
25 WT MCO High group ( $p<0.05$ , Kruskal-Wallis one-way analysis of variance followed by Dunn's  
26 pairwise multiple comparison procedures).

27

#### 28 *Mecp2 HET mice injected with AAV9-MCO do not show signs of long-term liver toxicity*

29 After phenotyping, the *Mecp2* HET MCO MED mice ( $n=5$ ) were sacrificed and their blood parameters  
30 and liver histology were analyzed (Figure 8). Compared to *Mecp2* HET mice injected with the AAV9-  
31 MCO vector that showed strongly elevated transaminase levels two weeks post-injection (Figure 1A-  
32 B), the *Mecp2* HET MCO group that was examined 30 weeks post vector administration did not show  
33 any significant changes in blood parameters (Figure 8A-F). When liver histology was examined using  
34 hematoxylin-eosin staining, we did not see any signs of liver damage in the *Mecp2* HET MCO (Figure

1 8I) compared to the WT or *Mecp2* HET groups (Figure 8G and H, respectively). Persistence of the  
2 transgene expression was also verified by immunostaining (Figure 8J-L). Because we could not see  
3 *Mecp2* staining in the WT and *Mecp2* HET mouse livers using immunofluorescence staining (data not  
4 shown), we used an amplification system coupled to the chromogenic immunodetection of *Mecp2* to  
5 increase the detection sensitivity. Using this technique, we could clearly see *Mecp2* staining in the  
6 WT group (Figure 8J) while there was faint and sparse staining in the *Mecp2* HET group (Figure 8K). In  
7 the *Mecp2* HET MCO livers, (Figure 8L), faint *Mecp2* staining was also present and did not seem to  
8 differ from the *Mecp2* HET group.

9 We further verified transgene clearance by assessing liver levels of *MCO* DNA and cDNA. We found  
10 little expression of *MCO* cDNA ( $2.85 \pm 1.05$  in HET AAV9-MCO MED, n=4, vs  $0.66 \pm 0.12$  in HET, n=3,  
11  $1 \pm 0.07$  in WT, n=3) and could not detect any *MCO* vector DNA, which indicates that the transgene  
12 had likely been cleared from the liver and is in agreement with the very low *Mecp2* staining observed  
13 in the *Mecp2* HET MCO livers (Figure 8L).

14

## 1 DISCUSSION

2 We and others have recently shown that gene therapy in Rett syndrome could be feasible as vector  
3 administration increased lifespan and ameliorated RTT phenotype in male *Mecp2*-deficient (*Mecp2*-  
4 KO) mice (Gadalla et al., 2013; Garg et al., 2013; Matagne et al., 2017). RTT mostly affects female  
5 patients and a lot of RTT symptoms (e.g. breathing deficits, motor and autonomic dysfunction) are  
6 present in female RTT mice, which makes them the genetically relevant RTT model to study (Katz et  
7 al., 2012). Given the fact that there is so far only one study reporting improvement in RTT symptoms  
8 after AAV9-mediated gene therapy in female RTT (or *Mecp2* HET) mice (Garg et al., 2013), we sought  
9 to investigate the effect of our previously characterized gene therapy vector (AAV9-MCO) in female  
10 *Mecp2* HET mice.

11 To test the potential therapeutic benefits of gene therapy, we proceeded to test its efficacy in 5-  
12 month-old *Mecp2* HET mice that were already presenting some deficits in breathing and  
13 spontaneous locomotor activity (Table 1 and 3). We decided not to compare the treated *Mecp2* HET  
14 mice to mice injected with vehicle instead of an AAV9-GFP vector because a nuclear GFP, which  
15 would be the best control, has been shown to cause cellular damages (Misteli and Spector, 1997). In  
16 addition, because of its potential toxicity (Ansari et al., 2016; Liu et al., 1999), we do not know if the  
17 GFP expression in itself cannot affect behavior as it was shown in *Drosophila* (Mawhinney and  
18 Staveley, 2011). As previously observed in the male *Mecp2* KO mice, there was some steady  
19 improvement in AAV9-MCO MED-treated *Mecp2* HET mice that reached significance by the end of  
20 the study. Improvement in spontaneous locomotor activity (open field test) was also observed as  
21 early as 8 weeks post-treatment but the effect on different parameters (distance, velocity, activity,  
22 vertical activity) was not observed simultaneously. We also monitored daily locomotor activity using  
23 a home cage video-tracking system and found that *Mecp2* HET mice already present decreased daily  
24 distance travelled at 5 months of age, which is in agreement with other studies reporting circadian  
25 alterations in different Rett mouse models (Li et al., 2015; Tsuchiya et al., 2015). Interestingly, a  
26 decrease in distance travelled did not become obvious before 12 months of age in the open field  
27 test, indicating that animals do not display the same behavior while they are in their home cage  
28 compared to forced tests (e.g. open field). Unlike findings by Garg et al, we did not see any  
29 improvement in the Rotarod test, which could be explained by the fact that we tested mice for  
30 sensorimotor function (3 trials on one day) while they evaluated motor skill learning (3 trials/day for  
31 3 consecutive days). Another difference concerned breathing function as we observed a consistent  
32 decrease in the number of apneas in treated *Mecp2* HET mice while Garg and colleagues reported  
33 inconclusive results (Garg et al., 2013). This discrepancy could be explained in part by the difference  
34 in the viral vector composition as Garg et al used a long *Mecp2* promoter and an endogenous  
35 *Mecp2e1* sequence while we used a short *Mecp2* promoter and an MCO sequence. This positive

1 effect of the AAV9-MCO vector on breathing dysfunction presents a high therapeutic interest since  
2 breathing dysfunctions are common in mouse models of RTT (Viemari et al 2005., Pratte et al., 2011).  
3 Moreover, in RTT patients breathing arrhythmia may be responsible for a quarter of the unexplained  
4 sudden death observed in RTT patients (Julu et al., 1997; Kerr et al., 1997; Tarquinio et al., 2018).

5  
6 Contrary to what we previously reported in the male *Mecp2*-KO mice, we found that *Mecp2* HET  
7 mice displayed a severe toxic reaction after AAV9-MCO administration. This side effect was dose-  
8 dependent, with the highest dose resulting in the death of half the injected mice while the medium  
9 dose had a reduced mortality (23%) and the low dose had no obvious side effects, but also no short-  
10 term beneficial effect on breathing dysfunction. As indicated by elevated levels of serum  
11 transaminases (AST, ALT), administration of AAV9-MCO at medium and high doses principally  
12 affected the liver, one of the organs for which AAV9 has a high tropism (Chen et al., 2015). Liver  
13 injury was then confirmed by disorganized liver architecture with the presence of  
14 cellular/lymphocyte infiltration and apoptotic cells, which is reminiscent of liver necrosis (Krishna,  
15 2017). In WT female mice, the administration of low or high doses of AAV9-MCO resulted in elevated  
16 transaminases but no toxic reaction as in the *Mecp2* HET mice. This, together with the fact that  
17 administration of high doses of the control AAV9-GFP vector did not cause any side effects in either  
18 *Mecp2* HET or WT mice, supports the idea that this toxic reaction is specific to the administration of  
19 AAV9-MCO in female RTT mice. These findings are reminiscent of the study by Gadalla and  
20 colleagues reporting a toxic reaction in the male *Mecp2* KO mice when they were administered a  
21 dose of  $10^{12}$ vg/mouse, which is one log above the therapeutic dose ( $10^{11}$ vg/mouse), while a dose of  
22  $10^{10}$ vg/mouse was inefficient (Gadalla et al., 2017). In agreement with our findings, they reported  
23 severe liver damage that was also due to the *Mecp2*-expressing vector only. These results are in  
24 contrast to those obtained by Garg et al. who used a dose of  $3 \times 10^{12}$  vg/mouse and did not report any  
25 deleterious side effects after administration in both male and female RTT mice (Garg et al., 2013).  
26 This discrepancy could be explained in part by the difference in the viral vector composition as Garg  
27 et al used a long *Mecp2* promoter and an endogenous *Mecp2e1* sequence while Gadalla et al used a  
28 short *Mecp2* promoter and a tagged human *MECP2* sequence (Gadalla et al., 2013), which is similar  
29 to the vector used here, except for the codon-optimized *Mecp2* sequence (MCO).

30 As stated above, the short-term toxic reaction to the AAV9-MCO seems to specifically occur in RTT  
31 female mice. Measurements of vector DNA and *Mco* transcripts in the liver of WT and *Mecp2* HET  
32 mice were not significantly different even though *Mecp2* HET mice levels tended to be higher (Figure  
33 6A-B). Interestingly, this trend then seemed to reverse itself, with *Mecp2* HET MCO mice displaying  
34 lower than expected *Mecp2* protein levels (Figure 6C). This led us to wonder whether an excessive

1 amount of *Mco* transcripts could have triggered the unfolded protein response (or UPR) pathway and  
2 be responsible for the toxic effect of the AAV9-MCO vector. The UPR pathway is a cyto-protective  
3 signaling pathway activated by endoplasmic reticulum (ER) stress and it has been shown to be  
4 triggered by various gene therapy vectors [reviewed in (Sen et al., 2014)]. Activation of UPR by  
5 accumulation of unfolded proteins in the ER leads to the production of chaperones and stress  
6 response proteins that will help reduce the protein load within the ER through degradation or to pro-  
7 apoptotic pathways /autophagy and cell death if the amount of unfolded protein in the ER is beyond  
8 its processing capacity. In agreement with a previous report (Balakrishnan et al., 2013), we did  
9 indeed find increased levels of *Chop* mRNA in the *Mecp2* HET MCO MED mice group. This increase  
10 was specific to the CHOP pathway and the AAV9-MCO vector since other BiP downstream elements  
11 (IRE1, ATF6) did not change and there were no significant changes in *Chop* mRNA after AAV9-GFP  
12 administration to *Mecp2* HET mice (data not shown). Increases in CHOP protein levels were also  
13 found in both WT and *Mecp2* HET mice injected with the vector but due to a high variability, it only  
14 reached significance in the WT MCO High group. Although there was an induction of CHOP after  
15 AAV9-MCO administration that could explain the severe liver damage in *Mecp2* HET, it does not  
16 explain why there is no liver damage in the WT mice. One hypothesis, is that, in addition to the UPR  
17 pathway, other degradation mechanisms may have been deficient in the *Mecp2* HET mice and  
18 involved in the toxic response observed. This could be the case of the autophagy pathway (Sbardella  
19 et al., 2017) and the Ubiquitin Proteasome System (UPS) (Sbardella et al., 2020) that both have been  
20 reported deregulated in RTT models. In agreement with this hypothesis is the fact that we did not  
21 find any liver damage nor detectable vector DNA or *Mecp2* overexpression in the liver of the HET  
22 MCO MED mice that were sacrificed at the end of the 30-week-long phenotypical study (Figure 7J-L).  
23 This would suggest that mice capable of safely degrading the excess of *Mecp2* occurring within 2  
24 weeks post vector administration would survive while those that could not because of a pre-existing  
25 liver condition, would suffer from severe toxic side effects.

26 In addition to defective protein degradation pathways, it was also reported that Rett patients  
27 suffered from metabolic deficits (Justice et al., 2013) and RTT mice displayed metabolic deficits and  
28 fatty liver disease (Kyle et al., 2016). In our study, we also found that untreated *Mecp2* HET mice  
29 presented significantly elevated ALT serum levels compared to the WT ones, which would argue for  
30 liver deficits in the *Mecp2* HET mice. This data suggest that liver function is altered in RTT, which may  
31 have led to a fragilized liver that was unable to cope with the consequences of massive vector  
32 transduction.

33 Another cause that could account for vector toxicity is the presence of contaminants (e.g. empty  
34 virions) in the viral preparation as previously reported in other cases (Wang et al., 2014). However,

1 the absence of side effects in simultaneously treated AAV9-MCO WT mice argues against this  
2 hypothesis.

3 To overcome this toxic effect, changes could be made to the vector itself or its payload to alter its  
4 liver tropism/expression and/or to the route of administration. The first option was investigated by  
5 Gadalla et al and showed that a combination of modified promoter, polyadenylation signal and  
6 capsid peptides lead to a vector with similar effect as the first generation vector without liver toxicity  
7 (Gadalla et al., 2017). A change in the administration route, i.e. intracisternal administration, of this  
8 new vector was also shown to diminish liver transduction but caused deleterious behavioral effects  
9 in both WT and RTT mice (Sinnott et al., 2017). In both cases, as already mentioned, it appeared that  
10 the usable vector dosage was between  $10^{10}$  and  $10^{12}$ vg/animal which indicates that the therapeutic  
11 range is very narrow and does not allow for mistakes. On the one hand, underestimating vector  
12 dosage would result in the absence of therapeutic effect and the production of neutralizing  
13 antibodies that would prevent the readministration of the same vector serotype unless coupled to  
14 immunosuppressant therapies (McIntosh et al., 2012). On the other hand, overestimating vector  
15 dosage could result in severe toxic shock or neurological side effects (Alvarez-Saavedra et al., 2010;  
16 Na et al., 2012).

17 It was recently reported that an AAV9 vector expressing a drastically truncated Mecp2 protein  
18 retaining the DNA binding domain and the NCoR/SMRT interaction domain was able to rescue male  
19 RTT mice without any side effect (Tillotson et al., 2017). There was also no side effect observed in the  
20 injected WT mice. As the authors mentioned, a shorter version of Mecp2 would mean a shorter  
21 sequence in the limited capacity of scAAV vector and therefore more room to add other regulatory  
22 elements. However, these experiments were carried out in neonatal mice that were injected  
23 intracranially and tests would need to be carried out in adult mice to ascertain the absence of side  
24 effect. In a very recent study, Luoni et al used a synthetic AAV, called AAV-PHP.eB, that was shown to  
25 preferentially target the brain (Deverman et al., 2016). Using this vector to deliver an instability-  
26 prone Mecp2, they showed a phenotypical rescue in both male and female RTT mice (Luoni et al.,  
27 2020). Although these results reinforce the idea that RTT could be amenable to gene therapy, the use  
28 of this vector is unfortunately restricted to studies using C57Bl/6J mice since its high brain tropism is  
29 lost when another mouse strain or nonhuman primates are injected (Hordeaux et al., 2018).

30 Overall, the preclinical results obtained so far clearly highlights the need for more research before  
31 gene therapy for RTT can safely move to the clinics. This is especially relevant in light of the recent  
32 death of 3 patients in the ASPIRO study, in which an AAV8-based vector was administered  
33 intravenously to children with X-linked myotubular myopathy. Not only is this vector displaying a  
34 high liver tropism similar to AAV9, but the deceased patients also seemed to present preexisting liver  
35 dysfunction (Shieh et al., 2020)

## 1 MATERIALS AND METHODS

### 2 **Animals**

3 The *Mecp2* heterozygous mice (B6,129P2(C)-*Mecp2* tm1-1Bird) were obtained from the Jackson  
4 Laboratory (Charles River, Chatillon-sur-Chalaronne, France) and maintained on a pure C57BL/6J  
5 background using male mice purchased from Charles River. Genotyping was performed by PCR-  
6 amplification following a previously described protocol (Miralvès et al., 2007). The animals were  
7 housed under a 12:12 h light / dark cycle (lights on at 07:00) and given free access to food and water.  
8 Experimental protocols were approved by the ethical committee of the Aix Marseille University and  
9 the committee of the Region Provence-Alpes-Côte d'Azur (Permit Number: 13-02910.02). All  
10 experiments were conducted in compliance with the European guidelines for the care and use of  
11 laboratory animals (EU directive 2010/63/EU), the *Haut Conseil des Biotechnologies* (authorization  
12 #6011) and the guide for the care and use of the laboratory animals of the French national institute  
13 for science and health (INSERM). All experiments were made to minimize animal suffering.

14

### 15 **Viral vector preparation and *in vivo* AAV injections**

16 Self-complementary recombinant pseudotyped AAV9 vectors were produced by the Vector Core at  
17 the University Hospital of Nantes ([www.atlantic-gene-therapies.fr](http://www.atlantic-gene-therapies.fr)) based on the protocol of Ayuso et  
18 al (Ayuso et al., 2010). The scAAV9 vectors used in this study have already been described in a  
19 previous publication (Matagne et al., 2017). Briefly, the vectors contained a cassette expressing a  
20 codon-optimized *Mecp2e1* version (experimental vector, AAV9-MCO) or GFP (control vector, AAV9-  
21 GFP) under the control of the short 264bp proximal *Mecp2* promoter (Adachi et al., 2005).

22 Five-month-old wild-type (WT) or heterozygous (HET) *Mecp2* female mice were sedated with a  
23 mixture of ketamine/xylazine (30mg/kg BW and 8mg/kg BW i.p., respectively) and intravenously  
24 injected with PBS only (control) or AAV9 vectors through the tail vein at three different doses: low  
25 ( $10^{11}$ ), medium ( $5 \times 10^{11}$ ) and high ( $10^{12}$ ) vg/mouse.

26

### 27 **Behavioral testing**

28 All mice were weighted once a week and tested 1 weeks before and 8, 16 and 30 weeks after AAV9-  
29 MCO administration. Sensorimotor function (Rotarod), spontaneous locomotor activity (open field)  
30 and breathing pattern (whole body plethysmography) were assessed following the protocol  
31 previously described (Matagne et al., 2017).

32 Homecage activity was assessed using the PhenoRack system (ViewPoint, Lyon, France). Mice were  
33 individually housed in large cages (24cm X 46cm) and given free access to food and water. After a  
34 habituation period (24h), mice were recorded by infrared cameras and the locomotor activity was

1 processed by the Videotrack software (Viewpoint, Lyon, France). Locomotor activity parameters  
2 (distance, activity duration and speed) were automatically generated by the software.

3

#### 4 **Tissue collection.**

5 Animals were euthanized with an overdose of sodium pentobarbital (100mg/kg BW, Ceva Santé  
6 Animale, La Ballastiere, France) and cardiac blood samples were collected before transcatheter  
7 perfusion with ice-cold PBS 1X (Sigma-Aldrich, Saint-Quentin Fallavier, France). The brain was rapidly  
8 dissected and sagittally cut in half; one half was then rapidly frozen in liquid nitrogen and the other  
9 half was post-fixed overnight in 4% paraformaldehyde (PFA, Sigma-Aldrich)-PBS 1X at 4°C. The right  
10 medial liver lobe was also dissected, frozen in liquid nitrogen and stored at -85°C until needed while  
11 the remaining liver lobes were post-fixed overnight in 4% PFA-PBS. After incubation in 4% PFA-PBS,  
12 the brain and liver samples were cryopreserved in a 20% sucrose-PBS 1X solution for 24h twice.  
13 Samples were then embedded in Tissue-Tek CRYO-OCT compound (Fisher Scientific, Illkirch, France)  
14 and serially sectioned at 20 or 40µm thickness on a Leica cryostat (VT1200s, Leica, Nanterre, France).  
15 Sections were kept at 4°C in cryoprotectant solution (30% sucrose, 30% ethylene glycol, 1%  
16 Polyvinylpyrrolidone 40 in 0.1M phosphate buffer) until processed for histology and immunostaining.

17

#### 18 **Blood chemistry analyses**

19 After 15 min at room temperature, samples were centrifuged at 4,500g RT for 10 min. The serum was  
20 recovered, frozen on dry ice and stored at -85°C until assay.

21 Samples were shipped on dry ice and assayed by the Mouse Metabolic Facility (MEF, Center for  
22 Integrative Genomics, UNIL, Lausanne, Switzerland) or the Mouse Clinical Institute (MCI, Illkirch,  
23 France).

24

#### 25 **RNA extraction, reverse transcription and quantitative real time qPCR**

26 Total RNA was isolated from liver samples using the Illustra RNeasy<sup>TM</sup> mini kit (GE Healthcare Life  
27 Sciences) according to the manufacturer's instruction. RNA concentration, quality and purity were  
28 verified by electrophoretic trace (NanoDrop, ThermoFisher Scientific).

29 One microgram of total RNA was retro-transcribed using the Superscript IV enzyme according to the  
30 manufacturer's instructions (Invitrogen, Life Technologies).

31 Quantitative assessment of *MCO* mRNA expression (forward primer 5'- CCTTCAGATCCAAGGTGGAA-  
32 3', reverse primer 5'- GGTCACGGTGAAGTCGAAGT-3'), *Bip* mRNA expression (forward primer 5'-  
33 CTGAGGCGTATTTGGGAAAG-3', reverse primer 5'- CTCATGACATTCAGTCCAGCA-3'), *CHOP* mRNA  
34 expression (forward primer 5'- GCGACAGAGCCAGAATAACA-3', reverse primer 5'-  
35 GATGCACTTCCTTCTGGAACA-3'), *IRE1* mRNA expression (forward primer 5'-

1 GGTCTTCGAAGCTACGATAAGG-3', reverse primer 5'- GGGCTGTTTGAATCAGTTATTA-3') and *ATF6*  
2 mRNA expression (forward primer 5'- GGACGAGGTGGTGTGTCAGAG-3', reverse primer 5'-  
3 GACAGCTCTTCGCTTTGGAC-3') were verified by quantitative real-time PCR using the LightCycler 480  
4 system (Roche). Each reaction was performed in a 20µl reaction containing 2µl of cDNA (diluted at  
5 1:20), 0.2 µM of each primer and 10µl of the SYBR Green I Master kit (Roche). Duplicates were run  
6 for each sample and the *Hmbs* gene (NM\_001110251.1, forward primer 5'-  
7 TCCCTGAAGGATGTGCCTAC-3', reverse primer 5'- CACAAGGGTTTTCCGTTT-3') was used as an  
8 internal control. Gene expression was obtained by the  $\Delta\Delta CT$  relative quantification method (Livak  
9 and Schmittgen, 2001) .

10 Primers were designed by the Universal ProbeLibrary Assay Design Center  
11 ([https://lifescience.roche.com/global\\_en/brands/universal-probe-library.html](https://lifescience.roche.com/global_en/brands/universal-probe-library.html))

12

### 13 **DNA extraction and quantitative real time qPCR**

14 Total DNA was isolated from liver and brain samples using the DNeasy Tissue and Blood kit (Qiagen,  
15 Courtaboeuf Cedex, France) according to the manufacturer's instruction. DNA concentration, quality  
16 and purity were verified by electrophoretic trace (NanoDrop, ThermoFisher Scientific).

17 Quantification of *AAV-MCO* DNA (forward primer 5'- GCCTTTTGCTGGCCTTTTGC-3', reverse primer 5'-  
18 GAGGCGGTTTGCATTTG-3') was made by quantitative real-time PCR using the LightCycler 480  
19 system (Roche). Each reaction was performed in a 20µl reaction containing 2µl of total DNA  
20 (50ng/µl), 0.2 µM of each primer and 10µl of the Luminaris Color HiGreen qPCR Master Mix (Thermo  
21 Scientific). Duplicates were run for each sample and the *Adora2b* gene (forward primer 5'-  
22 CCCAAGTGGGTGATGAATGT-3', reverse primer 5'- GGGGTTGACAACCTGAATTGG-3') was used as an  
23 internal control. Gene quantification was obtained by the  $\Delta\Delta CT$  relative quantification method (Livak  
24 and Schmittgen, 2001).

25

### 26 **Western blotting**

27 The tissue samples were homogenized in lysis buffer (20 mM Tris pH 7.5, 150 mM NaCl, 1% SDS, 1X  
28 Pierce Halt™ Protease Inhibitor Cocktail and 1X Pierce Halt™ Phosphatase Inhibitor Cocktail) by 5  
29 cycles of 30 sec sonication at high intensity using a Bioruptor (Diagenode, Seraing, Belgium). The  
30 protein extracts were then centrifuged for 10 min at maximum speed to pellet tissue debris and the  
31 protein concentration was determined using the Pierce BCA Protein assay (ThermoFisher Scientific).  
32 Thirty or 50µ g protein per lane were separated on an 4-20% pre-cast Tris-Glycine Novex midi gel  
33 (Thermofisher Scientific) and transferred on nitrocellulose membrane using the Trans-Blot® Turbo™  
34 blotting system (Bio-Rad, Marnes-la-Coquette, France). The same control sample was loaded on each  
35 gel to normalize the quantification. The membranes were rinsed in water and incubated with the

1 REVERT™ Total Protein Stain (LI-COR Biotechnology, Bad Homburg, Germany) for normalization  
2 purposes following the manufacturer's recommendations. The membrane was then blocked in  
3 freshly prepared Tris Buffer Saline Tween 20 buffer (TBST, pH 7.5, Tris 20mM, NaCl 137mM, 0,1%  
4 Tween 20) containing 5% semi-skimmed dry milk at room temperature for 1 h and incubated  
5 overnight in primary antibody (30µg/lane: Rabbit anti-MeCP2 (D4F3; 1:1,000, CST) or rabbit anti-  
6 CHOP (#5554; 1:400, CST) ; 50µg/lane: goat anti-GFP antibody 1:10,000, Abcam #ab6673) in TBST  
7 with mild agitation at 4°C. The membranes were washed 3 times in TBST for 5 min and incubated  
8 with an anti-mouse or anti-goat IRDye 800CW secondary antibody (LI-COR Biotechnology) diluted at  
9 1:10,000 in 5% nonfat dry milk TBST at room temperature for 1 h. After rinsing the membranes in  
10 TBST, the blots were visualized on an Odyssey infrared imager (LI-COR Biotechnology) or a ChemiDoc  
11 MP imaging system (Bio-rad).

12 Quantitation analysis (measurement of integrated pixel volume) was performed using the Image  
13 Studio™ Lite software (LI-COR Biotechnology) or the Image Lab software (Bio-rad).

14

## 15 **Histology**

### 16 H&E staining

17 Sections (40µm) were mounted on SuperFrost Plus slides (Fisher Scientific) and stored at -20°C until  
18 assay. Slides were left at room temperature for an hour and then rehydrated by successive  
19 incubation in 95% and 70% ethanol, and then water for 2 min before incubation in Vector  
20 hematoxylin solution (Eurobio) for 60 sec. After rinsing in water, the slides were incubated for 30 sec  
21 in Eosin Y solution (Sigma-Aldrich, # 318906, diluted 1:10 in 0.25% acetic acid and 70% ethanol) and  
22 then dehydrated by successive 2 min incubation in ethanol 70%, 95% and 100%. Sections were then  
23 cleared in xylene for 2 min and mounted in DPX mounting media (Fisher Scientific). Pictures were  
24 taken on 10X magnification (aperture 0.30 HCX PL FLUOTAR) on a Leica DM 5000B microscope  
25 equipped with a camera Leica (DFC 300 FX) and the magnification. Images were collected using the  
26 software Las V4.9. Exposition times, image processing and merging were done using the same  
27 parameter within each experiment.

28

### 29 Immunohistochemistry

30 After washing in dipotassium phosphate-buffered saline (KPBS) buffer (0.02 M, pH 7.4, 4 X 10min),  
31 free floating brain sections (40µm) were incubated for 30 min in 1% hydrogen peroxide-KPBS (Sigma-  
32 Aldrich, Saint-Quentin Fallavier, France) in order to block endogenous peroxidases. Liver sections  
33 (40µm) were incubated 20 min in 1% hydrogen peroxide-methanol. After 3 washes in KPBS, sections  
34 were incubated for 1 h at room temperature in blocking solution (2% normal donkey serum [Jackson

1 ImmunoResearch Europe, Ltd, Suffolk, UK], 0.3% Triton X-100, 0.02 M KPBS). Sections were then  
2 incubated with the primary antibody (rabbit anti-Mecp2, #3456, 1:500; Cell Signaling Technologies,  
3 Ozyme, St Quentin En Yvelines, France or goat anti-GFP, #ab6673, 1:500; Abcam, Cambridge, United  
4 Kingdom) diluted in blocking solution or in blocking solution only (NO AB sections) for 48 hours at 4°C  
5 under constant agitation. After washing 4 times in KPBS, sections were incubated 1 h in secondary  
6 antibody diluted at 1:200 in blocking solution (biotinylated donkey anti-goat IgG, #sc-2042 or anti-  
7 rabbit IgG, #sc2089; Santa Cruz Biotechnologies Inc., Heidelberg, Germany). Secondary amplification  
8 and detection were performed using the VectaStain ABC Elite Kit (#PK-6101; Vector Labs, Eurobio,  
9 Courtaboeuf, France) and the Vector VIP Peroxidase (HRP) Substrate Kit (#SK-4600) that were used  
10 according to the manufacturer recommendation. Immunostained sections were mounted on  
11 SuperFrost Plus slides (Fisher Scientific), dehydrated in ethanol (successive baths of 50%, 75%, 95%  
12 and 100% ethanol), cleared in Xylene and mounted in DPX mounting media (Fisher Scientific).  
13 Pictures were taken at 10X magnification (aperture 0.30 HCX PL FLUOTAR) on a Leica DM 5000B  
14 microscope equipped with a camera Leica (DFC 300 FX). Images were collected using the software  
15 Las V4.9. Exposition times, image processing and merging were done using the same parameter  
16 within each experiment.

17

#### 18 Immunohistofluorescence

19 Sections were washed in phosphate-buffered saline 1X (PBS) buffer (from PBS 10X, Gibco, Life  
20 Technologies) for 4 times (10 min), incubated in blocking solution (3% normal donkey serum [Jackson  
21 ImmunoResearch Europe, Ltd, Suffolk, UK], 0.3% Triton X-100, PBS 1X) for 1 h and transferred in  
22 primary antibody diluted in blocking solution or in blocking solution only (NO AB control sections) for  
23 48 h at 4°C. After washing the sections 4 times for 10 min, they were incubated for 1 h at room  
24 temperature with the secondary antibody diluted in blocking solution and then washed 4 more times  
25 in KPBS. Nuclei were stained by 5 min incubation with DAPI (0.4 µg/ml) followed by 2 rinses in KPBS.  
26 Sections were then mounted on glass slides, air-dried for 30 min and coverslipped with Shandon  
27 Immu-Mount (ThermoFisher Scientific). Primary antibodies were as follows: goat anti-GFP, (#ab6673,  
28 1:500; Abcam), rabbit anti-Mecp2 (#3456, 1:500; CST) and rabbit anti-Cleaved Caspase-3 (#9661,  
29 1:400; CST). Secondary antibodies (ThermoFisher Scientific) were all raised in donkey and were an  
30 anti-goat Alexa 488 (1:500, #A11055) and an anti-rabbit Alexa 596 (#R37117).

31 Pictures were taken on a Zeiss Apotome microscope (Carl Zeiss Microimaging, Jena, Germany) with  
32 objectives (10x/0.30 M27 DIC I EC Plan-Neofluar). Images were collected using the software Zen 2.3.  
33 Exposition times, image processing and merging were done using the same parameter within each  
34 experiment.

1 Semi-quantitative GFP measurement.

2 Using the Fiji software, fluorescence images of liver sections were converted to 8-bit format, then  
3 thresholded, and the density (integrated density) was measured with the Fiji *measuring tool*. Results  
4 obtained in AAV-GFP injected WT and Mecp2 HET groups were normalized to the uninjected WT  
5 group (background). All slides were analyzed with the experimenter blind for genotype and  
6 treatment.

7 TUNEL staining assay.

8 Liver apoptosis was measured in vivo with a TUNEL staining assay. Briefly, 2 WT (control), 2 HET MCO  
9 LOW, 2 HET MCO MED and 3 HET MCO HIGH mice were terminally sedated with an overdose of  
10 sodium pentobarbital (100mg/kg BW, Ceva Santé Animale, La Ballastiere, France) and livers were  
11 dissected after intracardiac perfusion of PBS 1X followed by 4% paraformaldehyde-PBS 1X and post-  
12 fixed by an overnight incubation with 4% paraformaldehyde-PBS 1X at 4°C. The liver was sectioned at  
13 20µm thickness on a Leica cryostat and mounted on SuperFrost Plus slides. The TUNEL assays were  
14 performed by using the Click-iT™ Plus TUNEL Assay for *in situ* apoptosis detection with Alexa 488  
15 Fluor™ dye (Invitrogen) according to the manufacturer's protocol. Nuclei were stained by 5 min  
16 incubation with DAPI (0.4 µg/ml) followed by 2 rinses in PBS 1X for 5min. Sections were then air-  
17 dried for 30 min and coverslipped with Shandon Immu-Mount (ThermoFisher Scientific).

18

19 **Statistical analysis**

20 All statistical analyses (unless specified otherwise) were performed using SigmaPlot 11 (Systat  
21 Software Inc., San Jose, CA). Comparison between 2 groups was analyzed by a Mann-Whitney rank  
22 sum test. Differences between groups were analyzed using a one-way ANOVA (normal distribution,  
23 equal variance) followed by the Holm-Sidak post-hoc tests or the Kruskal-Wallis one-way analysis of  
24 variance on ranks followed by Dunn's Method pairwise comparison procedure when the normality  
25 test failed. Data are expressed as means ± SEM and  $p < 0.05$  was considered significant for all tests.  
26 Two-way ANOVA and area under the curve (AUC) analyses were performed using GraphPad Prism for  
27 Windows/MacOS (GraphPad Software, La Jolla, California, USA, [www.graphpad.com](http://www.graphpad.com)). Word  
28 (Microsoft Office 365) was used to prepare the manuscript. Figures were designed using GraphPad  
29 Prism for Windows/MacOS. Radar charts in Figure 1 were plotted using the R software (v 4.0.0) and  
30 the ggradar package.

31

1 FUNDING

2 This work was supported by INSERM, Aix Marseille University, grants from the AFM-Téléthon  
3 (Strategic pole MNH Decrypt), Promex Stiftung Für Die Forschung, Rettsyndrome.org and Association  
4 Française du Syndrome de Rett (AFSR).

5

1 ACKNOWLEDGEMENTS

2 We thank the Vector Core ([www.atlantic-gene-therapies.fr](http://www.atlantic-gene-therapies.fr)) at the University Hospital of Nantes for  
3 the rAAV vector production, the imaging core facility, the animal phenotyping core facility for expert  
4 animal care, and Ana Borges-Correia, Adeline Spiga and Camille Fulachier for technical assistance.

5

1 CONFLICT OF INTEREST STATEMENT

2 The authors have no conflict of interest to disclose.

3

1 REFERENCES

- 2 Adachi, M., Keefer, E.W., Jones, F.S., 2005. A segment of the *Mecp2* promoter is sufficient to drive  
3 expression in neurons. *Hum. Mol. Genet.* 14, 3709–3722. doi:10.1093/hmg/ddi402
- 4 Alvarez-Saavedra, M., Carrasco, L., Sura-Trueba, S., Demarchi Aiello, V., Walz, K., Neto, J.X., Young,  
5 J.I., 2010. Elevated expression of MeCP2 in cardiac and skeletal tissues is detrimental for  
6 normal development. *Hum. Mol. Genet.* 19, 2177–2190. doi:10.1093/hmg/ddq096
- 7 Amir, R.E., Van den Veyver, I.B., Wan, M., Tran, C.Q., Francke, U., Zoghbi, H.Y., 1999. Rett syndrome  
8 is caused by mutations in X-linked MECP2, encoding methyl-CpG-binding protein 2. *Nat.*  
9 *Genet.* 23, 185–188. doi:10.1038/13810
- 10 Ansari, A.M., Ahmed, A.K., Matsangos, A.E., Lay, F., Born, L.J., Marti, G., Harmon, J.W., Sun, Z., 2016.  
11 Cellular GFP toxicity and immunogenicity: potential confounders in in vivo cell tracking  
12 experiments. *Stem Cell Rev* 12, 553–559. doi:10.1007/s12015-016-9670-8
- 13 Ayuso, E., Mingozi, F., Bosch, F., 2010. Production, purification and characterization of adeno-  
14 associated vectors. *Curr Gene Ther* 10, 423–436. doi:10.2174/156652310793797685
- 15 Balakrishnan, B., Sen, D., Hareendran, S., Roshini, V., David, S., Srivastava, A., Jayandharan, G.R.,  
16 2013. Activation of the cellular unfolded protein response by recombinant adeno-associated  
17 virus vectors. *PLoS One* 8, e53845. doi:10.1371/journal.pone.0053845
- 18 Chen, B.-D., He, C.-H., Chen, X.-C., Pan, S., Liu, F., Ma, X., Li, X.-M., Gai, M.-T., Tao, J., Ma, Y.-T., Yang,  
19 Y.-N., Gao, X.-M., 2015. Targeting transgene to the heart and liver with AAV9 by different  
20 promoters. *Clin. Exp. Pharmacol. Physiol.* 42, 1108–1117. doi:10.1111/1440-1681.12453
- 21 Cheng, T.-L., Chen, J., Wan, H., Tang, B., Tian, W., Liao, L., Qiu, Z., 2017. Regulation of mRNA splicing  
22 by MeCP2 via epigenetic modifications in the brain. *Sci. Rep.* 7, 42790.  
23 doi:10.1038/srep42790
- 24 Deverman, B.E., Pravdo, P.L., Simpson, B.P., Kumar, S.R., Chan, K.Y., Banerjee, A., Wu, W.-L., Yang, B.,  
25 Huber, N., Pasca, S.P., Gradinaru, V., 2016. Cre-dependent selection yields AAV variants for  
26 widespread gene transfer to the adult brain. *Nat. Biotechnol.* 34, 204–209.  
27 doi:10.1038/nbt.3440
- 28 Duque, S., Joussemet, B., Riviere, C., Marais, T., Dubreil, L., Douar, A.-M., Fyfe, J., Moullier, P., Colle,  
29 M.-A., Barkats, M., 2009. Intravenous administration of self-complementary AAV9 enables  
30 transgene delivery to adult motor neurons. *Mol. Ther.* 17, 1187–1196.  
31 doi:10.1038/mt.2009.71
- 32 Foust, K.D., Nurre, E., Montgomery, C.L., Hernandez, A., Chan, C.M., Kaspar, B.K., 2009. Intravascular  
33 AAV9 preferentially targets neonatal neurons and adult astrocytes. *Nat. Biotechnol.* 27, 59–  
34 65. doi:10.1038/nbt.1515
- 35 Gadalla, K.K.E., Bailey, M.E.S., Spike, R.C., Ross, P.D., Woodard, K.T., Kalburgi, S.N., Bachaboina, L.,  
36 Deng, J.V., West, A.E., Samulski, R.J., Gray, S.J., Cobb, S.R., 2013. Improved survival and  
37 reduced phenotypic severity following AAV9/MECP2 gene transfer to neonatal and juvenile  
38 male *Mecp2* knockout mice. *Mol. Ther.* 21, 18–30. doi:10.1038/mt.2012.200
- 39 Gadalla, K.K.E., Vudhironarit, T., Hector, R.D., Sinnett, S., Bahey, N.G., Bailey, M.E.S., Gray, S.J., Cobb,  
40 S.R., 2017. Development of a Novel AAV Gene Therapy Cassette with Improved Safety

- 1 Features and Efficacy in a Mouse Model of Rett Syndrome. *Mol. Ther. Methods Clin. Dev.* 5,  
2 180–190. doi:10.1016/j.omtm.2017.04.007
- 3 Garg, S.K., Lioy, D.T., Cheval, H., McGann, J.C., Bissonnette, J.M., Murtha, M.J., Foust, K.D., Kaspar,  
4 B.K., Bird, A., Mandel, G., 2013. Systemic delivery of MeCP2 rescues behavioral and cellular  
5 deficits in female mouse models of Rett syndrome. *J. Neurosci.* 33, 13612–13620.  
6 doi:10.1523/JNEUROSCI.1854-13.2013
- 7 Gray, S.J., Matagne, V., Bachaboina, L., Yadav, S., Ojeda, S.R., Samulski, R.J., 2011. Preclinical  
8 differences of intravascular AAV9 delivery to neurons and glia: a comparative study of adult  
9 mice and nonhuman primates. *Mol. Ther.* 19, 1058–1069. doi:10.1038/mt.2011.72
- 10 Guy, J., Gan, J., Selfridge, J., Cobb, S., Bird, A., 2007. Reversal of neurological defects in a mouse  
11 model of Rett syndrome. *Science (80-. )*. 315, 1143–1147. doi:10.1126/science.1138389
- 12 Hagberg, B., 1995. Rett syndrome: clinical peculiarities and biological mysteries. *Acta Paediatr.* 84,  
13 971–976.
- 14 Hocquemiller, M., Giersch, L., Audrain, M., Parker, S., Cartier, N., 2016. Adeno-Associated Virus-  
15 Based Gene Therapy for CNS Diseases. *Hum. Gene Ther.* 27, 478–496.  
16 doi:10.1089/hum.2016.087
- 17 Hordeaux, J., Wang, Q., Katz, N., Buza, E.L., Bell, P., Wilson, J.M., 2018. The Neurotropic Properties of  
18 AAV-PHP.B Are Limited to C57BL/6J Mice. *Mol. Ther.* 26, 664–668.  
19 doi:10.1016/j.ymthe.2018.01.018
- 20 Julu, P.O., Kerr, A.M., Hansen, S., Apartopoulos, F., Jamal, G.A., 1997. Immaturity of medullary  
21 cardiorespiratory neurones leading to inappropriate autonomic reactions as a likely cause of  
22 sudden death in Rett's syndrome. *Arch. Dis. Child.* 77, 464–465.
- 23 Justice, M.J., Buchovecky, C.M., Kyle, S.M., Djukic, A., 2013. A role for metabolism in Rett syndrome  
24 pathogenesis: New clinical findings and potential treatment targets. *Rare Dis.* 1, e27265.  
25 doi:10.4161/rdis.27265
- 26 Katz, D.M., Berger-Sweeney, J.E., Eubanks, J.H., Justice, M.J., Neul, J.L., Pozzo-Miller, L., Blue, M.E.,  
27 Christian, D., Crawley, J.N., Giustetto, M., Guy, J., Howell, C.J., Kron, M., Nelson, S.B., Samaco,  
28 R.C., Schaevitz, L.R., St Hillaire-Clarke, C., Young, J.L., Zoghbi, H.Y., Mamounas, L.A., 2012.  
29 Preclinical research in Rett syndrome: setting the foundation for translational success. *Dis.*  
30 *Model. Mech.* 5, 733–745. doi:10.1242/dmm.011007
- 31 Kerr, A.M., Armstrong, D.D., Prescott, R.J., Doyle, D., Kearney, D.L., 1997. Rett syndrome: analysis of  
32 deaths in the British survey. *Eur. Child Adolesc. Psychiatry* 6 Suppl 1, 71–74.
- 33 Krishna, M., 2017. Patterns of necrosis in liver disease. *Clin Liver Dis (Hoboken)* 10, 53–56.  
34 doi:10.1002/cld.653
- 35 Kyle, S.M., Saha, P.K., Brown, H.M., Chan, L.C., Justice, M.J., 2016. MeCP2 co-ordinates liver lipid  
36 metabolism with the NCoR1/HDAC3 corepressor complex. *Hum. Mol. Genet.* 25, 3029–3041.  
37 doi:10.1093/hmg/ddw156
- 38 Li, Q., Loh, D.H., Kudo, T., Truong, D., Derakhshesh, M., Kaswan, Z.M., Ghiani, C.A., Tsoa, R., Cheng, Y.,  
39 Sun, Y.E., Colwell, C.S., 2015. Circadian rhythm disruption in a mouse model of Rett syndrome  
40 circadian disruption in RTT. *Neurobiol. Dis.* 77, 155–164. doi:10.1016/j.nbd.2015.03.009

- 1 Liu, H.S., Jan, M.S., Chou, C.K., Chen, P.H., Ke, N.J., 1999. Is green fluorescent protein toxic to the  
2 living cells? *Biochem. Biophys. Res. Commun.* 260, 712–717. doi:10.1006/bbrc.1999.0954
- 3 Livak, K.J., Schmittgen, T.D., 2001. Analysis of relative gene expression data using real-time  
4 quantitative PCR and the 2(-Delta Delta C(T)) Method. *Methods* 25, 402–408.  
5 doi:10.1006/meth.2001.1262
- 6 Lombardi, L.M., Baker, S.A., Zoghbi, H.Y., 2015. MECP2 disorders: from the clinic to mice and back. *J.*  
7 *Clin. Invest.* 125, 2914–2923. doi:10.1172/JCI78167
- 8 Luoni, M., Giannelli, S., Indrigo, M.T., Niro, A., Massimino, L., Iannielli, A., Passeri, L., Russo, F.,  
9 Morabito, G., Calamita, P., Gregori, S., Deverman, B., Broccoli, V., 2020. Whole brain delivery  
10 of an instability-prone *Mecp2* transgene improves behavioral and molecular pathological  
11 defects in mouse models of Rett syndrome. *Elife* 9. doi:10.7554/eLife.52629
- 12 Lyst, M.J., Bird, A., 2015. Rett syndrome: a complex disorder with simple roots. *Nat. Rev. Genet.* 16,  
13 261–275. doi:10.1038/nrg3897
- 14 Matagne, V., Ehinger, Y., Saidi, L., Borges-Correia, A., Barkats, M., Bartoli, M., Villard, L., Roux, J.-C.,  
15 2017. A codon-optimized *Mecp2* transgene corrects breathing deficits and improves survival  
16 in a mouse model of Rett syndrome. *Neurobiol. Dis.* 99, 1–11. doi:10.1016/j.nbd.2016.12.009
- 17 Mawhinney, R.M.S., Staveley, B.E., 2011. Expression of GFP can influence aging and climbing ability in  
18 *Drosophila*. *Genet. Mol. Res.* 10, 494–505. doi:10.4238/vol10-1gmr1023
- 19 McIntosh, J.H., Cochrane, M., Cobbold, S., Waldmann, H., Nathwani, S.A., Davidoff, A.M., Nathwani,  
20 A.C., 2012. Successful attenuation of humoral immunity to viral capsid and transgenic protein  
21 following AAV-mediated gene transfer with a non-depleting CD4 antibody and cyclosporine.  
22 *Gene Ther.* 19, 78–85. doi:10.1038/gt.2011.64
- 23 Miralvès, J., Magdeleine, E., Joly, E., 2007. Design of an improved set of oligonucleotide primers for  
24 genotyping *MeCP2tm1.1Bird* KO mice by PCR. *Mol. Neurodegener.* 2, 16. doi:10.1186/1750-  
25 1326-2-16
- 26 Misteli, T., Spector, D.L., 1997. Applications of the green fluorescent protein in cell biology and  
27 biotechnology. *Nat. Biotechnol.* 15, 961–964. doi:10.1038/nbt1097-961
- 28 Müller, M., 2019. Disturbed redox homeostasis and oxidative stress: Potential players in the  
29 developmental regression in Rett syndrome. *Neurosci. Biobehav. Rev.* 98, 154–163.  
30 doi:10.1016/j.neubiorev.2018.12.009
- 31 Na, E.S., Nelson, E.D., Adachi, M., Autry, A.E., Mahgoub, M.A., Kavalali, E.T., Monteggia, L.M., 2012. A  
32 mouse model for *MeCP2* duplication syndrome: *MeCP2* overexpression impairs learning and  
33 memory and synaptic transmission. *J. Neurosci.* 32, 3109–3117.  
34 doi:10.1523/JNEUROSCI.6000-11.2012
- 35 Naidu, S., 1997. Rett syndrome: a disorder affecting early brain growth. *Ann. Neurol.* 42, 3–10.  
36 doi:10.1002/ana.410420104
- 37 Neul, J.L., Kaufmann, W.E., Glaze, D.G., Christodoulou, J., Clarke, A.J., Bahi-Buisson, N., Leonard, H.,  
38 Bailey, M.E.S., Schanen, N.C., Zappella, M., Renieri, A., Huppke, P., Percy, A.K., RettSearch  
39 Consortium, 2010. Rett syndrome: revised diagnostic criteria and nomenclature. *Ann. Neurol.*  
40 68, 944–950. doi:10.1002/ana.22124

- 1 Samaco, R.C., McGraw, C.M., Ward, C.S., Sun, Y., Neul, J.L., Zoghbi, H.Y., 2013. Female Mecp2(+/-)  
2 mice display robust behavioral deficits on two different genetic backgrounds providing a  
3 framework for pre-clinical studies. *Hum. Mol. Genet.* 22, 96–109. doi:10.1093/hmg/dds406
- 4 Samaco, R.C., Neul, J.L., 2011. Complexities of Rett syndrome and MeCP2. *J. Neurosci.* 31, 7951–  
5 7959. doi:10.1523/JNEUROSCI.0169-11.2011
- 6 Sbardella, D., Tundo, G.R., Campagnolo, L., Valacchi, G., Orlandi, A., Curatolo, P., Borsellino, G.,  
7 D’Esposito, M., Ciaccio, C., Cesare, S.D., Pierro, D.D., Galasso, C., Santarone, M.E., Hayek, J.,  
8 Coletta, M., Marini, S., 2017. Retention of mitochondria in mature human red blood cells as  
9 the result of autophagy impairment in rett syndrome. *Sci. Rep.* 7, 12297.  
10 doi:10.1038/s41598-017-12069-0
- 11 Sbardella, D., Tundo, G.R., Cunsolo, V., Grasso, G., Cascella, R., Caputo, V., Santoro, A.M., Milardi, D.,  
12 Pecorelli, A., Ciaccio, C., Di Pierro, D., Leoncini, S., Campagnolo, L., Pironi, V., Oddone, F.,  
13 Manni, P., Foti, S., Giardina, E., De Felice, C., Hayek, J., Curatolo, P., Galasso, C., Valacchi, G.,  
14 Coletta, M., Graziani, G., Marini, S., 2020. Defective proteasome biogenesis into skin  
15 fibroblasts isolated from Rett syndrome subjects with MeCP2 non-sense mutations. *Biochim.*  
16 *Biophys. Acta Mol. Basis Dis.* 165793. doi:10.1016/j.bbadis.2020.165793
- 17 Sen, D., Balakrishnan, B., Jayandharan, G.R., 2014. Cellular unfolded protein response against viruses  
18 used in gene therapy. *Front. Microbiol.* 5, 250. doi:10.3389/fmicb.2014.00250
- 19 Shieh, P.B., Bönnemann, C.G., Müller-Felber, W., Blaschek, A., Dowling, J.J., Kuntz, N.L., Seferian,  
20 A.M., 2020. Re: “moving forward after two deaths in a gene therapy trial of myotubular  
21 myopathy” by wilson and flotte. *Hum. Gene Ther.* 31, 787. doi:10.1089/hum.2020.217
- 22 Sinnott, S.E., Hector, R.D., Gadalla, K.K.E., Heindel, C., Chen, D., Zaric, V., Bailey, M.E.S., Cobb, S.R.,  
23 Gray, S.J., 2017. Improved MECP2 Gene Therapy Extends the Survival of MeCP2-Null Mice  
24 without Apparent Toxicity after Intracisternal Delivery. *Mol. Ther. Methods Clin. Dev.* 5, 106–  
25 115. doi:10.1016/j.omtm.2017.04.006
- 26 Sun, Y., Gao, Y., Tidei, J.J., Shen, M., Hoang, J.T., Wagner, D.F., Zhao, X., 2019. Loss of MeCP2 in  
27 immature neurons leads to impaired network integration. *Hum. Mol. Genet.* 28, 245–257.  
28 doi:10.1093/hmg/ddy338
- 29 Tarquinio, D.C., Hou, W., Neul, J.L., Berkmen, G.K., Drummond, J., Aronoff, E., Harris, J., Lane, J.B.,  
30 Kaufmann, W.E., Motil, K.J., Glaze, D.G., Skinner, S.A., Percy, A.K., 2018. The course of awake  
31 breathing disturbances across the lifespan in Rett syndrome. *Brain Dev.* 40, 515–529.  
32 doi:10.1016/j.braindev.2018.03.010
- 33 Tillotson, R., Selfridge, J., Koerner, M.V., Gadalla, K.K.E., Guy, J., De Sousa, D., Hector, R.D., Cobb, S.R.,  
34 Bird, A., 2017. Radically truncated MeCP2 rescues Rett syndrome-like neurological defects.  
35 *Nature* 550, 398–401. doi:10.1038/nature24058
- 36 Tsuchiya, Y., Minami, Y., Umemura, Y., Watanabe, H., Ono, D., Nakamura, W., Takahashi, T., Honma,  
37 S., Kondoh, G., Matsuishi, T., Yagita, K., 2015. Disruption of MeCP2 attenuates circadian  
38 rhythm in CRISPR/Cas9-based Rett syndrome model mouse. *Genes Cells* 20, 992–1005.  
39 doi:10.1111/gtc.12305
- 40 Wang, Z., Halbert, C.L., Lee, D., Butts, T., Tapscott, S.J., Storb, R., Miller, A.D., 2014. Elimination of  
41 contaminating cap genes in AAV vector virions reduces immune responses and improves

- 1 transgene expression in a canine gene therapy model. *Gene Ther.* 21, 363–370.
- 2 doi:10.1038/gt.2014.4
- 3

1 LEGENDS TO FIGURES

2 Figure 1: Administration of AAV9-MCO improves some phenotypical abnormalities in *Mecp2* HET  
3 female mice. **A:** Study protocol schematic. Five-month-old *Mecp2* HET female mice and their wild-  
4 type controls were submitted to phenotypical analysis (open field, Rotarod, plethysmography) 1  
5 week before and 8, 16 and 30 weeks after viral vector administration at a medium (MED) dose  
6 ( $5 \times 10^{11}$  vg/mouse). **B-C:** Radar chart exemplifying the performance of each group across  
7 representative phenotypic variables at 1 week before viral vector administration (**B**) and 30 weeks  
8 after viral vector administration (**C**). While there was no significant difference between the HET and  
9 the HET MCO MED groups before treatment (**B**), all parameters showed improvement in the HET  
10 MCO MED group compared to the HET one (**C**). **D:** Throughout the study, *Mecp2* HET presented a  
11 significantly higher number of apneas compared to the WT group (\* : WT vs HET). This difference was  
12 also seen in the treated MCO group before injection (& : WT vs HET MCO MED). After vector  
13 administration, there was a decrease in the number of apneas that reached significance by 16 weeks  
14 post-vector administration (\$ : HET vs HET MCO MED). **E:** Sensorimotor function was analyzed by the  
15 rotarod test. There was no significant difference between groups at the beginning of the study while  
16 *Mecp2* HET mice displayed a decrease latency to fall compared to the wild type (WT) group at  
17 ulterior times. *Mecp2* HET mice did not show any improvement in sensorimotor function after vector  
18 administration. **F-I:** Spontaneous locomotor activity was assessed with the open field test.  
19 Throughout the study, HET mice showed significantly different performances in distance (**F**) velocity  
20 (**G**), activity (**H**) and vertical activity (**I**) compared to the WT group. These defects in locomotor  
21 activity parameters seemed to be slightly improved in the treated MCO group as their performance  
22 in distance (**F**) velocity (**G**) and activity (**H**) was not significantly different from the WT. Vertical  
23 activity was significantly improved in *Mecp2* HET MCO MED compared to untreated *Mecp2* HET. \*  
24 :  $p < 0.05$ , \*\* :  $p < 0.01$ , \*\*\* :  $p < 0.001$ , Two-way ANOVA followed by Tukey's multiple comparisons test (\*  
25 : WT vs HET, & : WT vs HET MCO MED, \$ : HET vs HET MCO MED) ns: non-significant difference. (n=13  
26 for WT, 11 for HET and 5 for HET AAV9-MCO).

27 Figure 2: Administration of AAV9-MCO tends to normalize home cage activity in treated *Mecp2* HET  
28 female mice. The home cage activity of *Mecp2* HET female mice injected with a medium (MED) dose  
29 ( $5 \times 10^{11}$  vg/mouse) of AAV9-MCO was continuously monitored over a 24 hour period 30 weeks after  
30 administration and their locomotor activity assessed. **A:** In Five-month-old mice, there is a significant  
31 decrease in the daily total distance travelled by *Mecp2* HET mice compared to WT controls (\*\*  
32  $p = 0.003$ , Mann-Whitney Rank Sum Test). Scatter plots show values for each animal and mean  $\pm$  SEM  
33 are represented by vertical bars. (n): number of animals per group. **B:** Compared to wild-type mice  
34 (WT), *Mecp2* HET female mice (HET) travelled shorter distance throughout the day. This behavioral

1 abnormality was improved in *Mecp2* HET mice injected with a medium dose of AAV9-MCO vector  
2 (HET MCO MED,  $5 \times 10^{11}$  vg/mouse) when examining home cage activity 30 weeks post treatment. **C:**  
3 Area under the curve (AUC) analyses showed that *Mecp2* HET mice significantly travelled less than  
4 WT mice and that treatment improved this deficit. Scatter plots show values for each animal and  
5 mean  $\pm$  SEM are represented by vertical bars. (n): number of animals per group. # : $p < 0.05$ , Kruskal-  
6 Wallis one way analysis of variance followed by Dunn's pairwise multiple comparison procedures.

7 Figure 3: Administration of AAV9-MCO causes liver damages in both MCO-injected *Mecp2* HET and  
8 WT mice. Five-month-old *Mecp2* HET female mice and their wild-type controls were administered  
9 with AAV9-MCO at a low, medium (MED) or high dose ( $10^{11}$ ,  $5 \times 10^{11}$  or  $10^{12}$  vg/mouse, respectively).  
10 Blood samples were collected 2 weeks post vector administration. Liver damage markers (ALT, AST)  
11 were measured in WT and *Mecp2* HET mice injected with AAV9-MCO. ALT levels were significantly  
12 increased in both high dose MCO-injected *Mecp2* HET and WT mice and surprisingly in low dose  
13 MCO-injected WT mice (**A**). AST levels were significantly increased in both low and high dose MCO-  
14 injected WT mice, and in both medium and high dose MCO-injected *Mecp2* HET mice (**B**). Scatter  
15 plots show values for each animal and mean  $\pm$  SEM are represented by vertical bars, # : $p < 0.05$ ,  
16 Kruskal-Wallis one way analysis of variance followed by Dunn's pairwise multiple comparison  
17 procedures. (n): number of animals per group. Liver integrity was assessed by hematoxylin and eosin  
18 (H&E) staining (**C-H**). Compared to WT (**C**) and *Mecp2* HET mice (**D**), the livers of medium and high  
19 dose AAV9-MCO injected HET (**F,H**) showed clear liver damage characterized with massive  
20 lymphocyte infiltration (star) and apoptotic cells (arrows). AAV9-MCO injected WT mice (**E,G**) did not  
21 show any liver damage even with the high dose (**G**). Scale bar=100 $\mu$ m

22 Figure 4: Administration of a high dose of AAV9-MCO causes apoptosis in the liver of *Mecp2* HET  
23 mice.

24 **A-F:** TUNEL staining of the mouse liver after injection of increasing AAV9-MCO dose in *Mecp2* HET  
25 mice. Images are representative pictures showing TUNEL staining (green color) in (**A**) positive control  
26 using WT section treated with DNase; (**B**) WT control; (**C**) HET control; (**D**) HET MCO LOW ( $10^{11}$   
27 vg/mouse); (**E**) HET MCO MED ( $5 \times 10^{11}$  vg/mouse) and (**F**) HET MCO HIGH ( $10^{12}$  vg/mouse) mice. Cells  
28 nuclei are counterstained by DAPI staining (blue color). Positive staining is observed in the HET MCO  
29 HIGH group.

30 **G-K:** Cleaved caspase 3 staining of the mouse liver after injection of increasing AAV9-MCO dose in  
31 *Mecp2* HET mice. Images are representative pictures showing cleaved caspase 3 staining (red color)  
32 in (**G**) WT control; (**H**) HET control; (**I**) HET MCO LOW ( $10^{11}$  vg/mouse); (**J**) HET MCO MED ( $5 \times 10^{11}$

1 vg/mouse) and **(K)** HET MCO HIGH ( $10^{12}$  vg/mouse) mice. Positive staining is observed in the HET  
2 MCO MED and HIGH groups.

3 The scale bar represents 200  $\mu\text{m}$ . (n=2 for WT, n=2 for the HET placebo, n=3 for HET MCO LOW, n= 2  
4 for HET MCO MED and n=3 for the HET MCO HIGH group).

5 Figure 5: Administration of the control GFP vector results in liver transgene expression. The AAV9-  
6 GFP vector **(B,D)** was administered to five-month-old WT**(A-B)** and *Mecp2* HET mice **(C-D)** at a high  
7 dose ( $10^{12}$  vg/mouse) and transgene expression was verified 2 weeks after injection by  
8 immunofluorescence and western blotting. In the AAV9-GFP groups **(B, D)**, GFP expression was  
9 visible in the liver after immunostaining while there was no visible GFP in the controls **(A,C)**. GFP  
10 staining is shown in green and nuclei are counterstained by DAPI in blue. Scale bar=100 $\mu\text{m}$ . Western  
11 blot quantification **(E)** showed that GFP expression was significantly higher in the *Mecp2* HET GFP  
12 group compared to the WT GFP one (\*\* p=0.009, Mann-Whitney rank sum test). Representative  
13 western blot images with the GFP protein stained in green are shown below each graph. Scatter plots  
14 show values for each animal and mean $\pm$ SEM are represented by vertical bars. (n): number of animals  
15 per group.

16 Figure 6: Administration of increasing doses of therapeutic vector results in dose-dependent liver  
17 transgene protein expression. The AAV9-MCO vector was administered to five-month-old WT and  
18 *Mecp2* HET mice at a low, medium (MED) or high dose ( $10^{11}$ ,  $5 \times 10^{11}$  or  $10^{12}$  vg/mouse, respectively)  
19 and transgene transduction and expression in the liver was verified 2 weeks after injection by  
20 quantitative PCR, quantitative RT-PCR, and western blotting. Administration of increasing doses of  
21 AAV9-MCO results in increasing liver AAV transduction in WT and *Mecp2* HET mice **(A)**. AAV9-MCO  
22 vector DNA was significantly detected in livers of both medium and high dose MCO-injected WT  
23 mice. *Mecp2* HET mice display significant MCO vector DNA levels after high dose administration. *Mco*  
24 cDNA expression was significantly increased in the *Mecp2* HET MCO MED and HIGH groups in a dose-  
25 dependent manner **(B)**. Curiously, it was not the case in the MCO-injected WT mice with a significant  
26 increase in the WT MCO LOW and HIGH groups only. Western blot quantification **(C)** showed a dose-  
27 dependent increase in *Mecp2* expression after vector administration in both *Mecp2* HET and WT  
28 groups. Representative western blot images with the *Mecp2* protein stained in black are shown next  
29 to the graph. Scatter plots show values for each animal and mean $\pm$ SEM are represented by vertical  
30 bars. \*\* : p<0.01 \*\*\* : p<0.001 1-way ANOVA followed by Holm Sidak post-hoc test. # :p<0.05,  
31 Kruskal-Wallis one way analysis of variance followed by Dunn's pairwise multiple comparison  
32 procedures. (n): number of animals per group.

1 Figure 7: Administration of the AAV9-MCO vector triggers the activation of the UPR cascade. Five-  
2 month-old *Mecp2* HET female mice and their wild-type controls were administered with AAV9-MCO  
3 at a low, medium (MED) or high dose ( $10^{11}$ ,  $5 \times 10^{11}$  or  $10^{12}$  vg/mouse, respectively) and sacrificed 2  
4 weeks after vector administration for post-mortem analysis. Using quantitative real-time PCR, we  
5 measured the mRNA levels of *Bip* (Binding immunoglobulin protein, **A**), the master regulator of the  
6 UPR pathway, and three downstream elements: *Chop* (C/EBP homologous protein, **B**), *IRE1* (inositol-  
7 requiring enzyme 1, **C**) and *ATF6* (activating transcription factor 6, **D**). **A**: There was a trend in higher  
8 levels of *Bip* mRNA in both WT and *Mecp2* HET injected mice. **B**: In the liver of *Mecp2* MCO MED HET  
9 mice, there was a significant increase in *CHOP* mRNA levels. A smaller, but significant increase in  
10 *CHOP* mRNA levels was also observed in the MCO HIGH WT group. **C**: There were no changes in *IRE1*  
11 mRNA levels in the AAV9-MCO group. Although *IRE1* mRNA levels in *Mecp2* AAV9-MCO HET mice  
12 were significantly different from the control group, post-test comparison between groups did not  
13 reach significance ( $p=0.049$ , 1-way ANOVA followed by Holm Sidak post-hoc test). **D**: There were no  
14 significant changes in *ATF6* mRNA levels after AAV9-MCO administration in WT or *Mecp2* HET mice.  
15 Western blot quantification (**E**) showed an increase in CHOP expression after vector administration in  
16 both *Mecp2* HET and WT groups. Representative western blot images with the CHOP protein stained  
17 in black are shown next to the graph. LC = Loading Control. # : $p < 0.05$ , Kruskal-Wallis one way analysis  
18 of variance followed by Dunn's pairwise multiple comparison procedures. Scatter plots with bar show  
19 values for each animal and mean  $\pm$  SEM are represented by vertical bars. (n): number of animals per  
20 group.

21 Figure 8: Long-term effect of AAV9-MCO administration on *Mecp2* HET mice. Five-month-old *Mecp2*  
22 HET female mice were administered with a medium (MED) AAV9-MCO dose ( $5 \times 10^{11}$  vg/mouse) and  
23 underwent phenotypical analysis. Mice were sacrificed at the end of the 30 week-long phenotyping  
24 study and blood samples were collected at that time. Markers for Liver (ALT, AST, respectively **A** and  
25 **B**), heart (CK, **C**), kidney (creatinine, urea, respectively **D** and **E**), and general tissue damage (LDH, **F**)  
26 were measured in WT, *Mecp2* HET (HET) and *Mecp2* HET mice injected with a medium dose of AAV9-  
27 MCO vector (HET MCO MED,  $5 \times 10^{11}$  vg/mouse). In the *Mecp2* HET MCO MED group, there was no  
28 significant difference in all the tested parameters compared to the WT and *Mecp2* HET groups.  
29 Scatter plots show values for each animal and mean  $\pm$  SEM are represented by vertical bars. (n):  
30 number of animals per group. (**G-I**) Liver integrity was assessed by hematoxylin and eosin (H&E)  
31 staining. Compared to WT (**G**) and *Mecp2* HET (**H**), the liver of *Mecp2* HET MCO MED mice (**I**) did not  
32 show any gross abnormality. (**J-L**) Persistence of transgene expression was assessed by *Mecp2*  
33 immunostaining. Compared to the WT mouse liver (**J**), *Mecp2* staining was very faint in the *Mecp2*  
34 HET (**K**) and *Mecp2* HET MCO MED (**L**) livers. Scale bar=100 $\mu$ m.

1

2 TABLES

3 Table 1: Breathing parameters obtained by whole-body plethysmography of 5-month-old *Mecp2* HET  
4 mice

	WT (13)	HET (16)
Hyperventilation	7356 ± 510	8100 ± 683
Ventilation	3029 ± 296	3211 ± 339
Hypoventilation	116 ± 26	140 ± 27
Apneas	17 ± 4	86.44 ± 14.7***
Mean frequency	185 ± 3	200 ± 4**
Variability	52 ± 1.5	57.5 ± 1.7*

5

6 The breathing frequency is the number of inspiration cycles per minute. Apnea, hypoventilation,  
7 ventilation and hyperventilation are breathing cycles determined by the cycle duration: more than 1s  
8 without breathing between two cycles (apneas), 0.7–1 s (hypoventilation), 0.3-0.7s (ventilation) and  
9 0.3-0s (hyperventilation) and are expressed as the number of cycle/hour. The breathing variability  
10 was calculated as the mean standard variability

11 \* $P < 0.05$ , \*\* $P < 0.01$ \*\*\* $P < 0.001$ , Mann-Whitney rank sum test. Values are expressed as mean ± SEM.  
12 (n): number of animals/group.

13

14

1 Table 2

2

	WT (13)	HET (11)	HET MCO MED (5)
Hyperventilation	5651 ± 1091	9115 ± 1616	6926 ± 1698
Ventilation	4556 ± 405	2201 ± 659 *	3544 ± 1008
Hypoventilation	228 ± 53	112 ± 28	119 ± 54
Apneas	41 ± 9	78.02 ± 8.61 <sup>+,&amp;</sup>	34.81 ± 11.35
Mean frequency	196 ± 2	214 ± 6 <sup>+</sup>	199 ± 6
Variability	54.5 ± 1.7	59.4 ± 1.8	58 ± 2

3

4 Treatment of 5-month-old HET mice with a medium dose of AAV9-MCO (5X10<sup>11</sup> vg/mouse) rescues  
5 the number of apneas when comparing them to untreated HET mice at 30 weeks post-injection

6 The breathing frequency is the number of inspiration cycles per minute. Apnea, hypoventilation,  
7 ventilation and hyperventilation are breathing cycles determined by the cycle duration: more than 1s  
8 without breathing between two cycles (apneas), 0.7–1 s (hypoventilation), 0.3-0.7s (ventilation) and  
9 0.3-0s (hyperventilation) and are expressed as the number of cycle/hour. The breathing variability  
10 was calculated as the mean standard variability

11 <sup>+</sup> *P*<0.05, Kruskal-Wallis test with Dunn's multiple comparison of the *Mecp2* HET vs WT.

12 <sup>&</sup> *P*<0.05, Kruskal-Wallis test with Dunn's multiple comparison of the *Mecp2* HET vs the AAV9-MCO  
13 HET group.

14 <sup>\*</sup> *P*<0.05 *Mecp2* HET vs WT groups, 1-way ANOVA with Holm-Sidak post-hoc test. Values are  
15 expressed as mean ± SEM. (n): number of animals/group.

16

17

1 Table 3: Phenotypic assessment of 5-month-old *Mecp2* HET mice

2

Behavioral assay	WT (13)	HET (16)
Rotarod (latency to fall in sec)	90.75 ± 16.95	70.27 ± 14.4
Open field Activity (% of total time)	93 ± 0.1	81.5 ± 0.4**
Open field Distance travelled (in cm)	13925.75 ± 682.7	11491.1 ± 1303.2
Open field velocity (in cm/s)	12.44 ± 0.5	11.54 ± 1.1
Open field Vertical activity (events/test)	173.46 ± 9.4	97.3 ± 5.95***

3

4

5 \*\**P*=0.003, \*\*\**P*<0.001, Mann-Whitney rank sum test.

6

1 Table 4 : summary of all animal treatment and study.

2

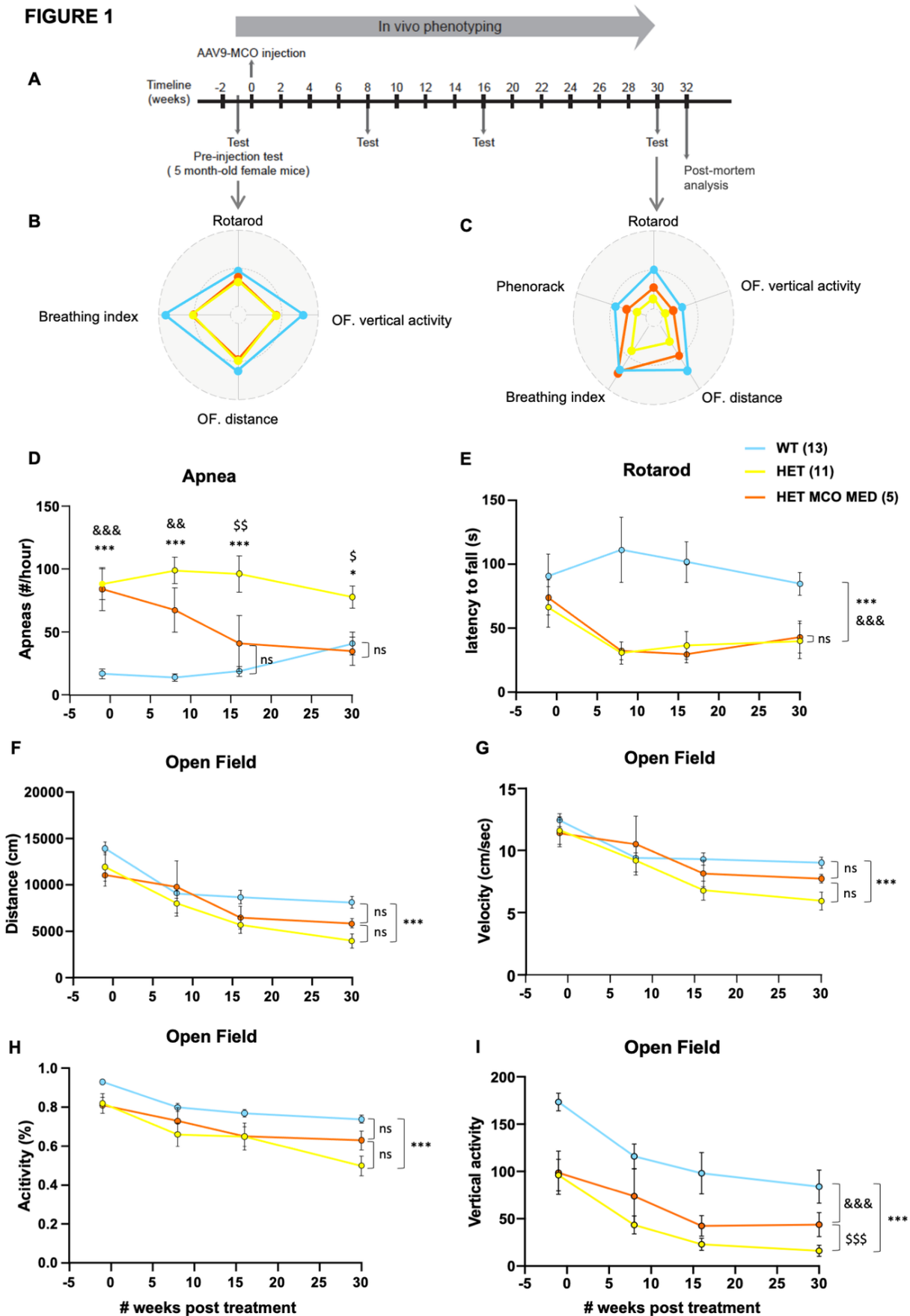
Mice group (n)		Vector	Study length (weeks)	Study protocol (n)	Miscellaneous
# 1	HET (5)	MCO MED	32	Behavioral testing at 8, 16 and 30wks PI (1) Sacrifice at 32wks PI, collection of brain and liver for histological analysis	None
# 2	HET (4)	MCO HIGH	32	Id.	2 MCO HIGH mice found dead
# 3	HET (5) HET (5)	MCO MED MCO HIGH	2	Blood chemistry Post-mortem analyses	- 3 MCO HIGH mice found dead - 1 mouse MCO MED found dead - 2 MCO HIGH and 2 MCO MED mice euthanized b/c of severe side effect. Blood and tissue samples collected at the time of sacrifice
# 4	HET (6) HET (3) HET (4)	MCO LOW MCO MED MCO HIGH	2	Blood chemistry Post-mortem analyses	No adverse effect observed
#5	WT (5) WT (6) WT (4)	MCO LOW MCO MED MCO HIGH	2	Blood chemistry Post-mortem analyses	No adverse effect observed
#6	HET (8) WT (7)	AAV9-GFP	2	Blood chemistry Post-mortem analyses	No adverse effect observed

3

4 Five-month-old wild-type (WT) or *Mecp2* heterozygous (HET) female mice were injected with the  
 5 AAV9-MCO at three different doses (LOW:  $10^{11}$  , MED:  $5 \times 10^{11}$  ,HIGH:  $10^{12}$  vg/mouse) or AAV9-GFP at  
 6 a dose of  $10^{12}$  vg/mouse. Long-term study lasted 30 weeks post-injection (PI) and consisted in the  
 7 phenotypical study of all animal according to the protocol depicted in Figure 1A. Short-term study  
 8 lasted 2 weeks PI.

9

10

**FIGURE 1**

**FIGURE 2**

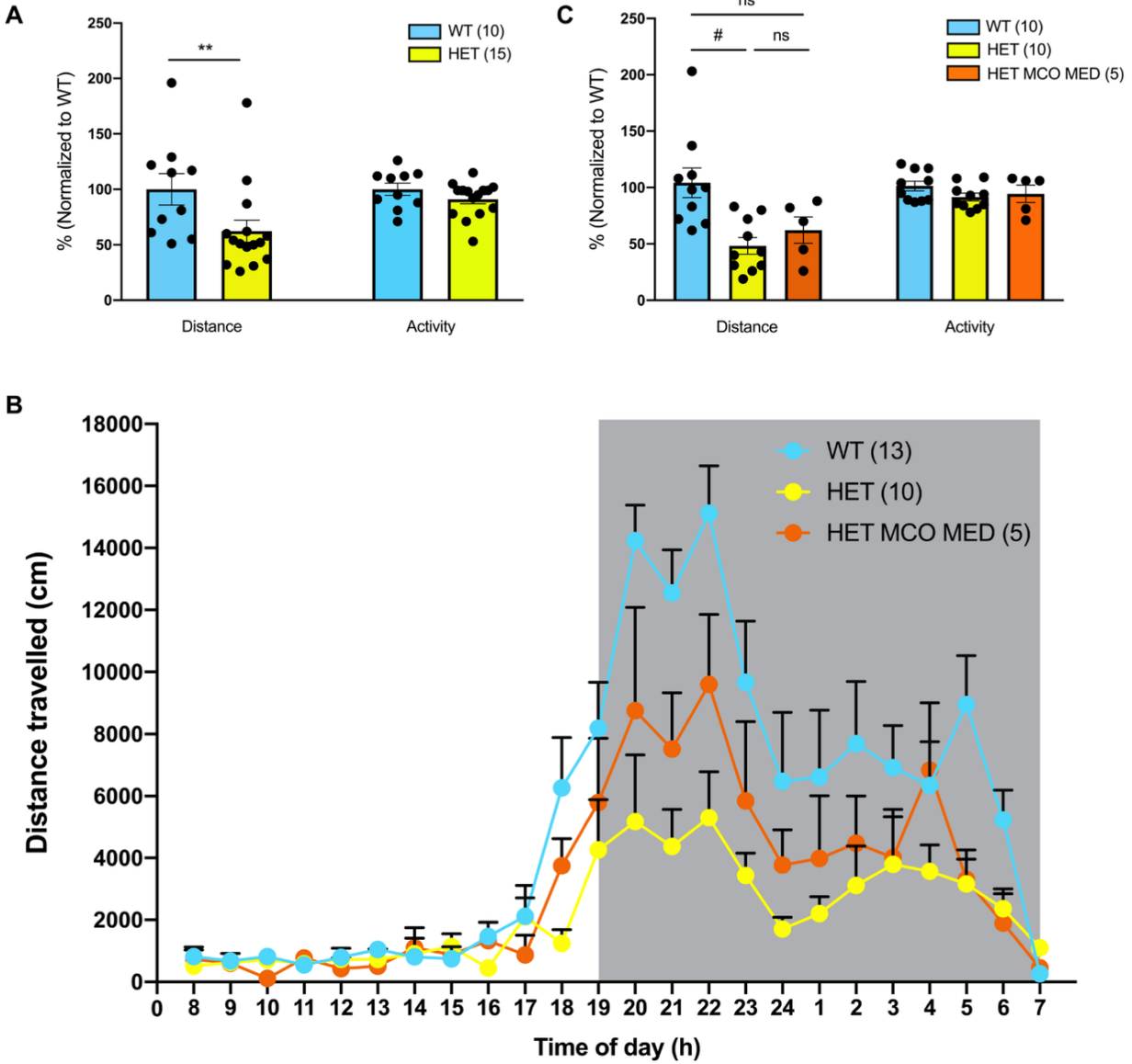


**FIGURE 3**

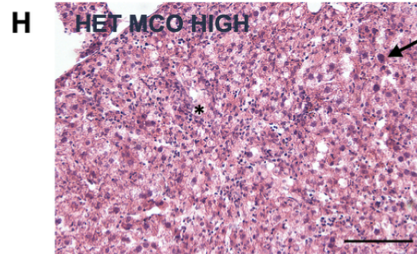
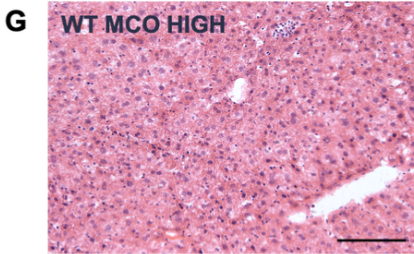
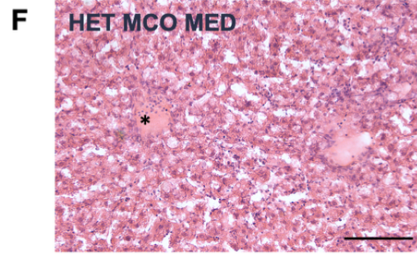
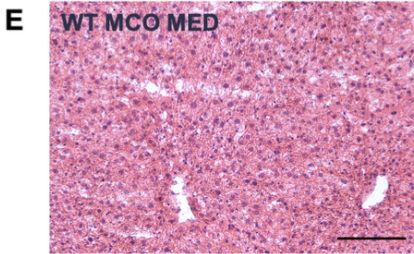
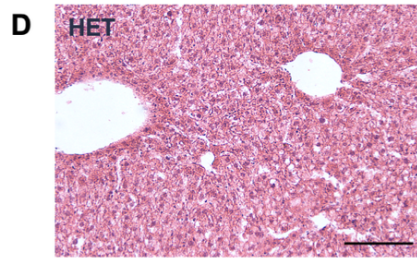
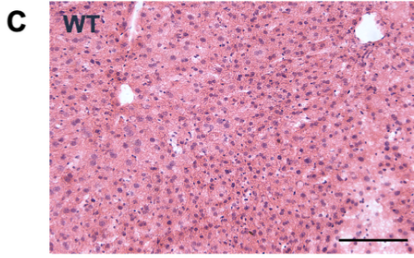
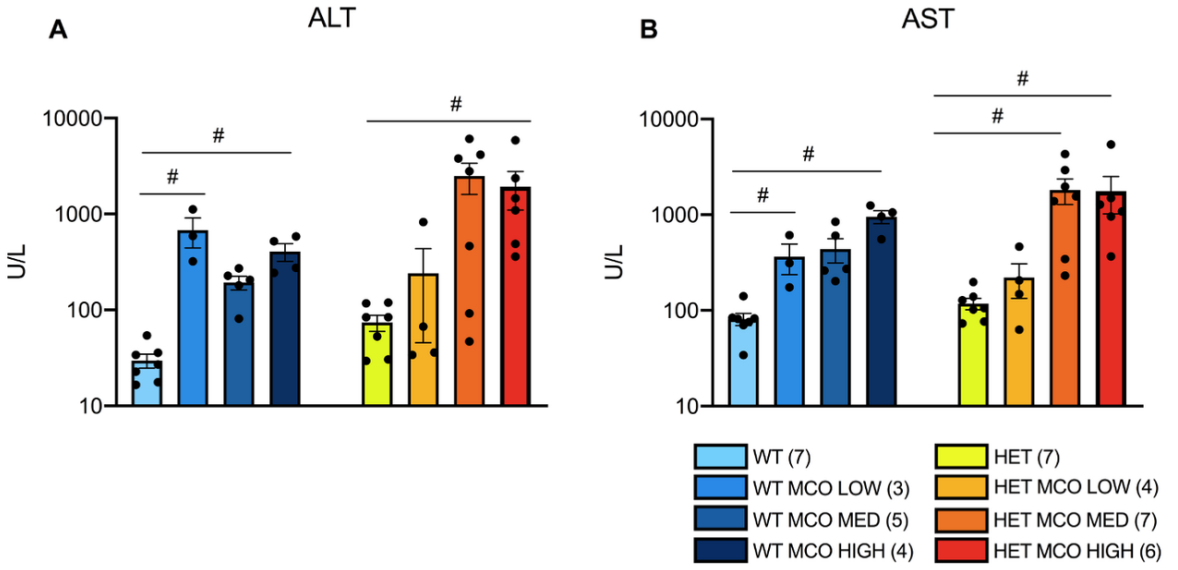


FIGURE 4

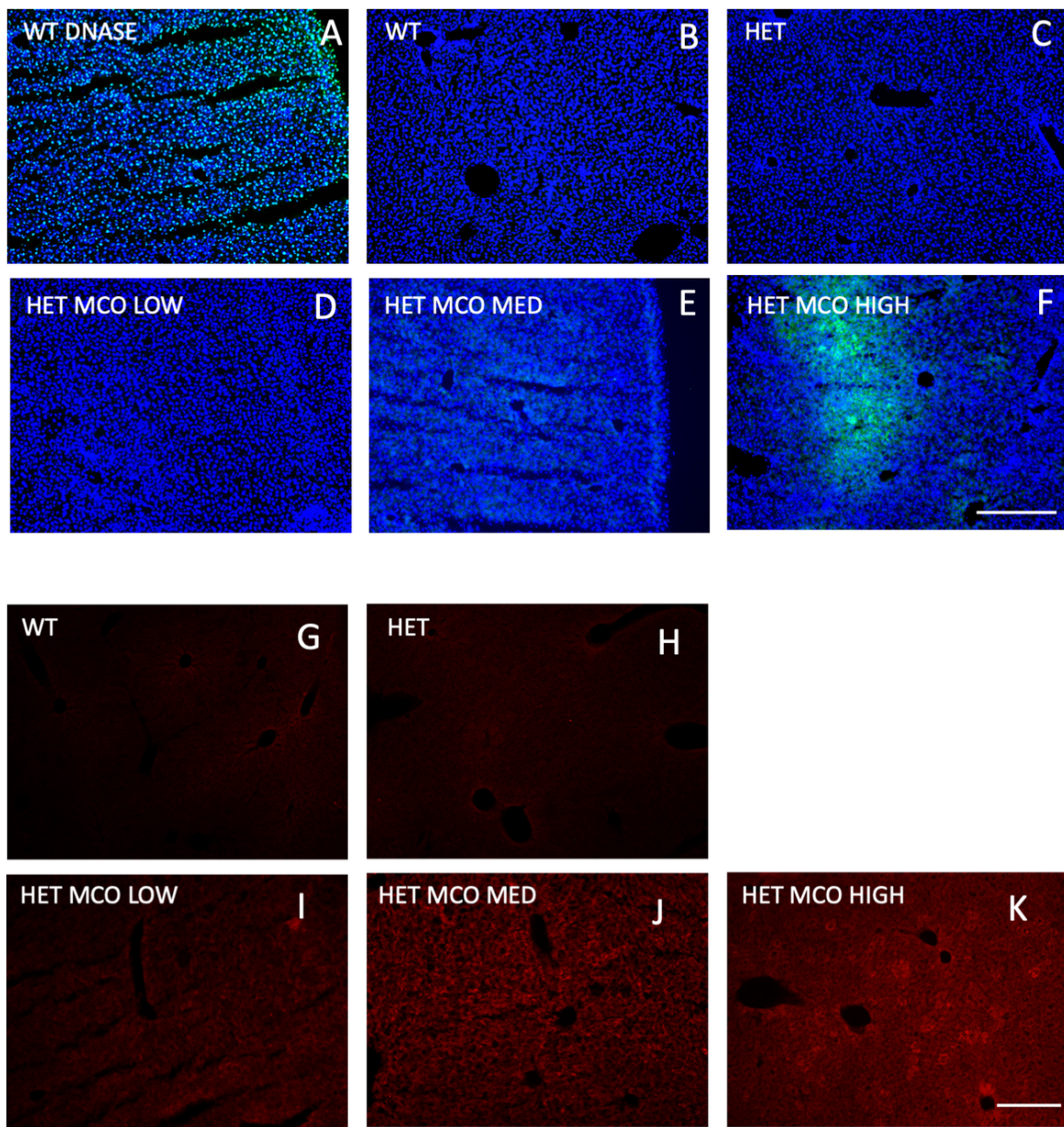
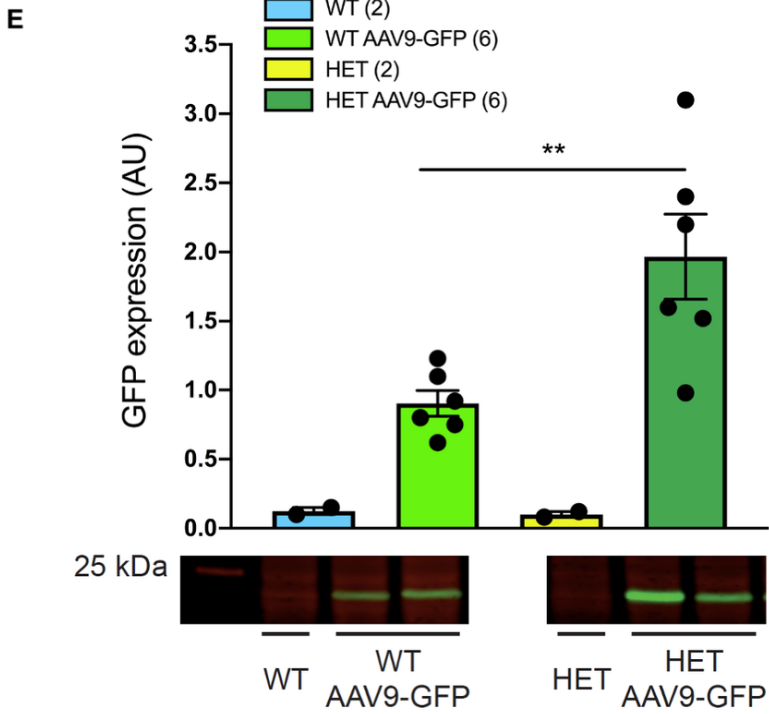
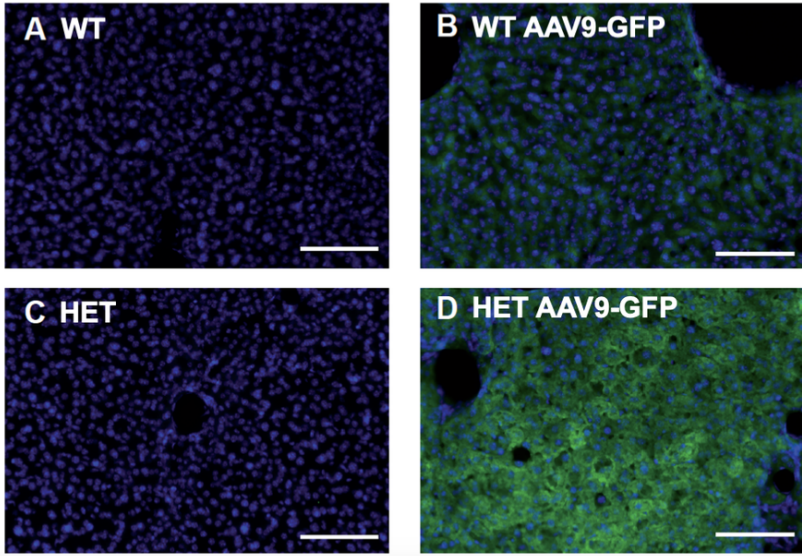
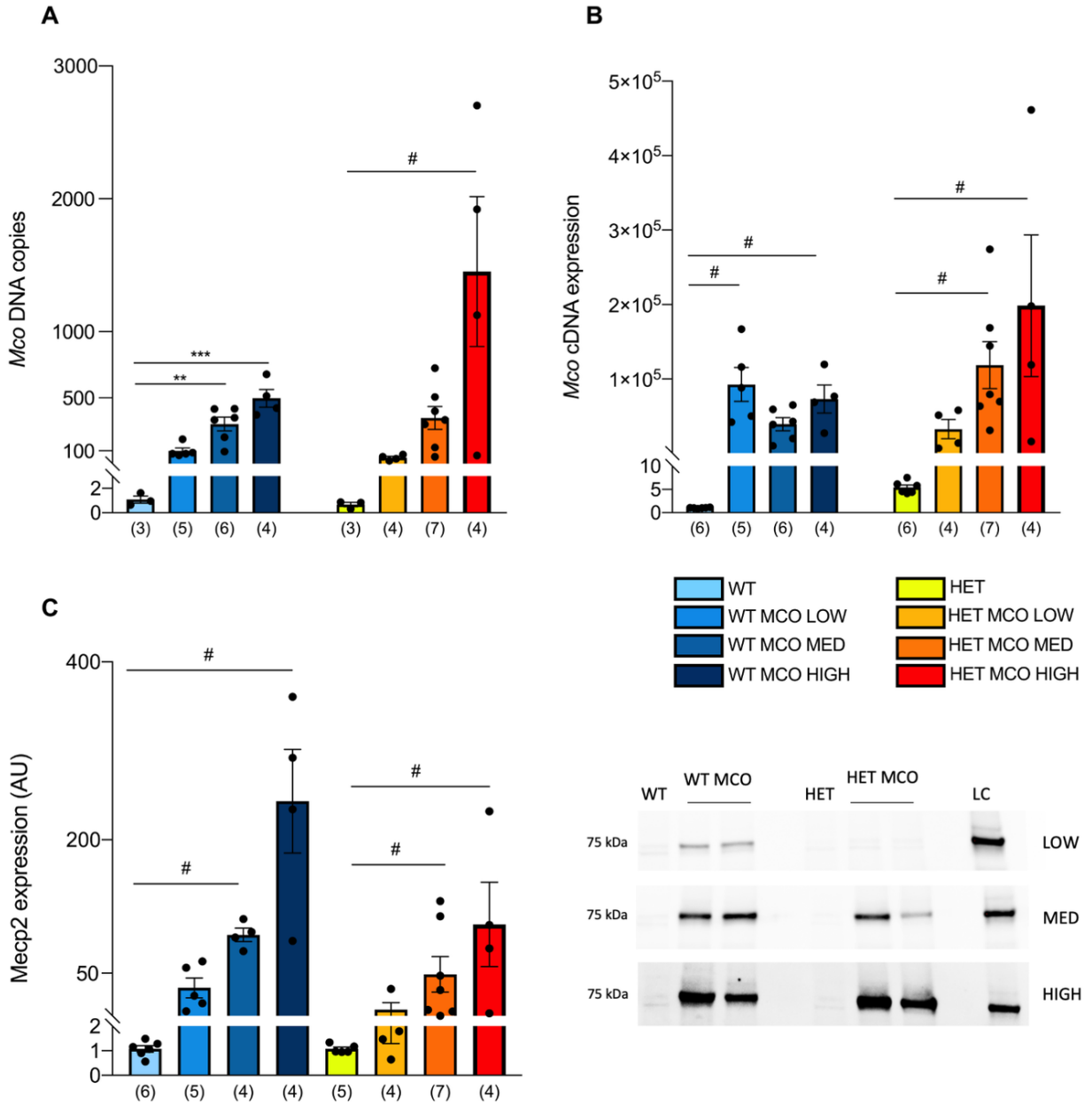


FIGURE 5

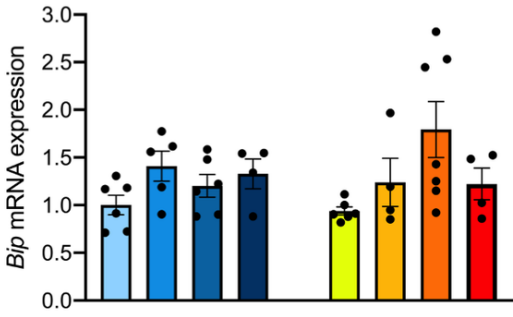


**FIGURE 6**

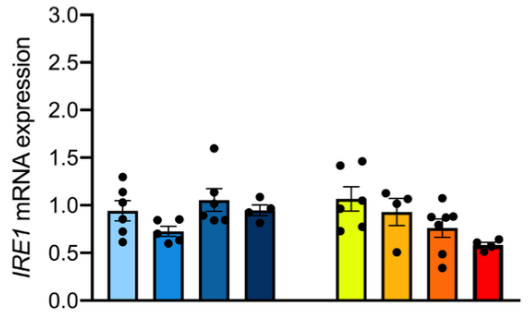


**FIGURE 7**

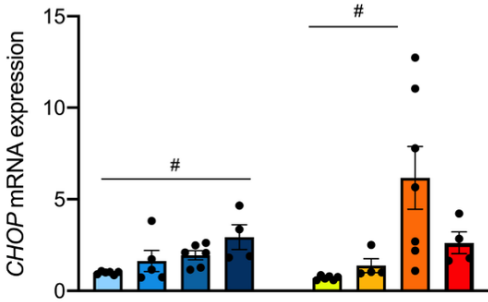
**A**



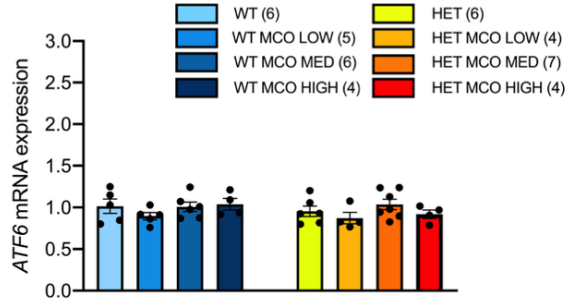
**C**



**B**



**D**



**E**

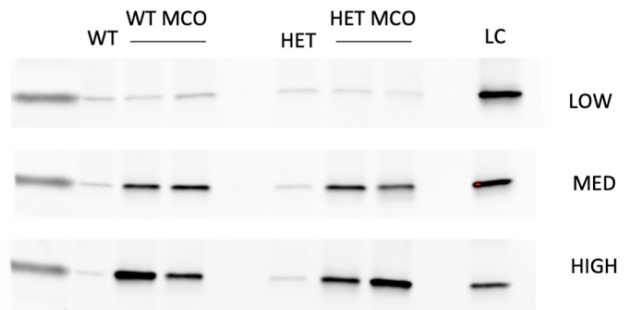
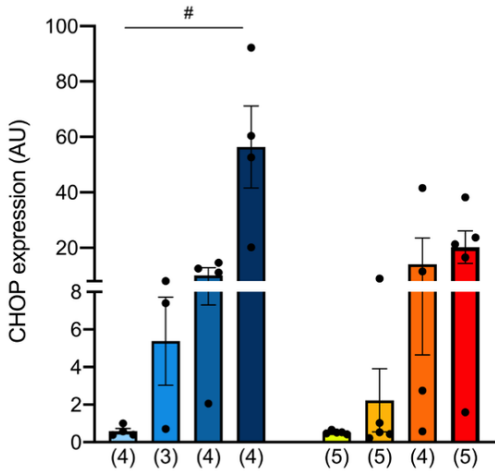


**FIGURE 8**

